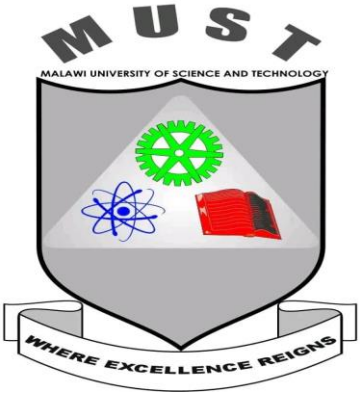


EFFICIENCY OF BAOBAB SHELL DERIVED ACTIVATED CARBON IN THE REMOVAL OF INORGANIC ANIONS FROM DOMESTIC WASTEWATER

ALICE CHILACHILA (WQM-002-21)

Thyolo, Malawi

Dissertation submitted to Ndata School of Climate and Earth Sciences of the Malawi University of Science and Technology in partial fulfilment of the requirements for the Bachelor of Science degree in Water Quality and Management

May, 2026

PROPOSAL APPROVED BY:

SUPERVISOR:

MR H. YAPUWA Signature: 

ASSESSOR:

Title, Initials, Name Signature: _____

DISCLAIMER

This document describes work undertaken as part of a programme of study at Ndata School of Climate and Earth Sciences of the Malawi University of Science and Technology. All views and opinions expressed therein remain the sole responsibility of the author, and do not necessarily represent those of the school.

COPYRIGHT STATEMENT

This copy of the dissertation has been supplied on condition that anyone who consults it is understood to recognize that its copyright rests with its author and that no quotation from the dissertation and no information derived from it may be published without acknowledgement.

ABSTRACT

The release of untreated or poorly treated domestic wastewater containing inorganic anions such as nitrate and sulphate causes major environmental and public health problems in Malawi. Conventional wastewater treatment systems have not been able to effectively remove dissolved inorganic anions; at the same time, advanced treatment technologies are expensive to implement in low resource settings. This study focused on developing a low-cost adsorbent produced from baobab fruit shells to remove inorganic anions from domestic wastewater. Phosphoric acid (H_3PO_4) was used for one-step chemical activation followed by carbonization at 700°C to produce activated carbon. Measured physicochemical characteristics included the carbon yield, moisture content, volatile matter, ash content, pH_pzc, iodine number, pore volume and porosity of the produced adsorbent. Using batch adsorption experiments with wastewater samples obtained from the Malawi University of Science and Technology wastewater treatment facility, batch studies assessed how well the BFS-AC removed nitrate and sulphate by examining the influences of pH, adsorbent dose and contact time. The BFS-AC produced had a carbon yield of 70.3%, low moisture (1.4%), moderate ash (9.27%) and a high iodine number (922.18 mg/g) showing a good mix of porosity and capacity for adsorption. In addition, the pH_pzc of the BFS-AC was 4.01, indicating that the adsorbent was acidic in nature. Evaluation revealed that the activation of baobab fruit shell for adsorption purposes would make it more efficient in the removal of nitrate and sulphate compared to raw baobab fruit shell. Furthermore, at pH 7.0, activated carbon provided the highest removal efficiencies of nitrate and sulphate as follows: removal efficiencies of 90.45% for nitrate and 88.14% for sulphate were achieved using an optimum dosage of 2.0 g of activated carbon and contact time of 90 minutes. Nitrate and sulphate were best described by pseudo-second-order models with R^2 of 0.9595 for sulphate and R^2 of 0.9621 for the nitrate adsorptions. This suggests that there was considerable surface interaction during adsorption process. The Freundlich isotherm provided the best fit for nitrate adsorption with the R^2 value of 0.9779 which indicated that heterogeneous adsorption occurred, while the Langmuir isotherm represented the best fit for sulphate adsorption supported by high R^2 value of 0.9655 indicating that monolayer-type adsorption occurred at relatively evenly-distributed active sites. The activated carbon also improved the clarity of

wastewater through substantial reduction of the electrical conductivity and total dissolved solids. Therefore, activated carbon (BFS-AC) produced from baobab fruit shell is a cost-effective, sustainable and highly effective adsorbent for removing inorganic anions from domestic wastewater. This research demonstrates that locally produced agricultural residue can be used as an alternative to costly wastewater treatment systems promoting sustainable water management, pollution control, and the recovery of resources within Malawi.

ACKNOWLEDGEMENTS

I sincerely thank the Almighty God for granting me guidance, wisdom, strength, and good health throughout the course of this research, making the successful completion of this study possible.

I would like to express my deepest gratitude to my supervisor, Mr. H. Yapuwa, for his continuous support, valuable guidance, encouragement, and constructive feedback, which greatly contributed to the successful completion and quality of this work.

My heartfelt appreciation also goes to my parents, Mr. and Mrs. Chilachila, and my siblings for their unwavering support, prayers, and encouragement throughout my academic journey. I am equally grateful to my close friends, Mr. Malijani and Miss Jacqueline Chauwa, for their support and motivation during this study.

Table of Contents

DISCLAIMER iii

COPYRIGHT STATEMENT iv

ACRONYMS/ABBREVIATION xi

LIST OF FIGURES xii

LIST OF TABLES xiii

CHAPTER 1: INTRODUCTION 1

1.1 Background information 1

1.2 Problem statement 2

1.3 Study objectives 2

Main objective 2

1.4 Research questions 3

1.5 Scientific significance of the study 3

CHAPTER 2: LITERATURE REVIEW 4

2.1 Domestic wastewater and inorganic anions 4

Water scarcity and wastewater reuse for irrigation 4

2.2 Limitations of conventional wastewater treatment 5

2.3 Adsorption and activated carbon 6

Activating Agents — Implications for BFS-AC and Anion Removal 8

2.4 Baobab fruit shell as a sustainable adsorbent 9

2.4.1 Availability and Socio-Environmental Rationale 9

2.4.2 Lignocellulosic composition and implications on AC production 9

2.4.3 Empirical performance and efficiencies 9

2.4.4 Yield considerations 10

2.5 Research Gap 10

CHAPTER 3: METHODOLOGY 11

3.0 Introduction 11

3.1 Study area 11

3.1 Research design 12

3.2 Sampling design 12

3.3 Materials and methods 13

3.3.0 Measurement of wastewater parameters 13

3.6 Data analysis 22

CHAPTER 4: RESULTS AND DISCUSSION 23

4.0 introduction 23

5.1 production and physicochemical characterisation of bfs-ac 23

5.1 carbon yield of activated carbon 23

5.1 moisture content 24

5.1.3 volatile content 25

4.1.4 ash content 26

5.1.4 ph at point of zero charge 28

5.2 micropore and surface characteristics 29

4.2.1 iodine number 29

4.2.2 pore volume and porosity 30

4.3 validation of activation: performance comparison with raw baobab shell precursor 31

4.4 wastewater clarification and adsorption performance of bfs-ac 34

4.4.2 adsorption performance: effect of ph, dosage, and contact time 35

4.4.2.3 effect of contact time 40

4.5 adsorption kinetics 42

4.5.1 pseudo-first-order model 43

4.5.2 pseudo-second-order model 44

4.6 adsorption isotherms..... 46

4.6.1 langmuir isotherm 47

4.6.2 freundlich isotherm 48

4.6.3 comparison of isotherm models..... 50

4.7comparative performance with published studies 51

CHAPTER 5: CONCLUSION AND RECOMMENDATIONS 53

REFERENCE.....56

APPENDIX.....63

ACRONYMS/ABBREVIATION

AC	Activated Carbon
BOD	Biochemical oxygen demand
BFS	Baobab fruit shell
BFS-AC	Baobab fruit shell Activated Carbon
COD	Chemical oxygen demand
H_3PO_4	Phosphoric acid
KOH	Potassium Hydroxide
PHpzc	pH at point zero charge
PH	Power of hydrogen
TDS	Total dissolved solids
TSS	Total suspended solids
WHO	World Health Organization
WWTP	Wastewater Treatment Plant
PFO	Pseudo-first order
PSO	pseudo-second order
RE	Removal efficiency
$ZnCl_2$	Zinc Chloride

LIST OF FIGURES

Figure 1: Map of MUST CAMPUS.....12
Figure 2: Flow diagram showing the preparation stages of BFS-AC 15
Figure 3: Graphic diagram of raw adsorbent preparation 15
Figure 4: Batch experiment setup for evaluation of pH effect on anion removal using RB 21
Figure 5: Batch experiment setup for evaluation of pH effect on anion removal using BFS-AC 21
Figure 6: pH at point of zero charge of BFS-AC 29
Figure 7: Effect of solution pH on removal of NO_3^- and SO_4^{2-} by BFS-AC 36
Figure 8: Effect of adsorbent dosage on removal of NO_3^- and SO_4^{2-} by BFS-AC 39
Figure 9: Effect of contact time on removal of NO_3^- and SO_4^{2-} by BFS-AC 41
Figure 10: Showing plot for PSO for (a) sulphate and (b) nitrate..... 45
Figure 11: Langmuir adsorption isotherms for (a) sulphate and (b) nitrate..... 48
Figure 12: Freundlich adsorption isotherms for (a) Nitrate and (b) Sulphate 50
Figure 13: Calibration curves for (a) nitrate and (b) sulphate 62
Figure 14: Stages in BFS-AC production.....71
Figure 15: Characterisation and adsorption experiment 71

LIST OF TABLES

Table 1: Mean influent and effluent of inorganic anions and removal efficiencies from selected WWTP in Malawi 6
Table 2: Wastewater parameters and methods that were used 14
Table 3: The production and yield parameters 23
Table 4: Moisture content of BFS-AC 25
Table 5: Volatile matter of BFS-AC 25
Table 6: Ash content of BFS-AC 27
Table 7: Iodine number of BFS-AC 30
Table 8: Pore volume and porosity of BFS-AC 30
Table 9: Comparison of physicochemical properties for Raw BFS and BFS-AC 31
Table 10: Nitrate removal efficiency for Raw BFS vs BFS-AC 33
Table 11: Sulphate removal efficiency for Raw BFS vs BFS-AC 33
Table 12: Initial and post-treatment physicochemical properties of wastewater 34
Table 13: Statistical analysis of the effect of solution pH on NO_3^- and SO_4^{2-} removal 36
Table 14: Effect of adsorbent dosage on nitrate and sulphate removal 38
Table 15: Effect of contact time on nitrate and sulphate removal 40
Table 16: Calculated q_t values at each contact time for nitrate and sulphate 43
Table 17: Pseudo-first-order linearisation data, ln ($q_e - q_t$) versus t 44
Table 18: Pseudo-second-order linearisation data t/q_t versus t 44
Table 19: Comparison of PFO and PSO kinetic model parameters 45
Table 20: Equilibrium adsorption data from multi-concentration isotherm experiments 46
Table 21: Langmuir isotherm parameters for NO_3^- and SO_4^{2-} adsorption onto BFS-AC .. 48
Table 22: Freundlich isotherm parameters for NO_3^- and SO_4^{2-} adsorption onto BFS-AC. 49
Table 23: Comparative adsorption performance for nitrate and sulphate removal 51
Table 24: Results on effect of solution pH on NO3- removal 62
Table 25: Results on effect of solution pH on SO42- removal 63
Table 26: Results on effect of adsorbent dosage on NO3- removal 63
Table 27: Results on effect of adsorbent dosage on SO42- removal 64

CHAPTER 1: INTRODUCTION

1.1 Background information

Domestic wastewater is a major contributor to water pollution in both urban and rural areas. It contains a mixture of organic matter, pathogens, and dissolved inorganic anions such as chloride, nitrate, phosphate, and sulphate (Adonadaga, 2019). While these anions are naturally occurring and essential in small concentrations for ecological balance, plant growth, and human health, excessive amounts pose serious environmental and health risks. Elevated nitrates and phosphates cause eutrophication, leading to algal blooms, oxygen depletion, and loss of aquatic biodiversity (avi & Kumari, 2024), while excessive chlorides and sulphates may contribute to corrosion, altered water taste, and adverse health conditions.

In Malawi, many wastewater treatment facilities are either inadequate or absent, resulting in untreated or partially treated domestic wastewater being discharged into the environment (Mdolo, 2017). Conventional treatment methods such as sedimentation, biological stabilization ponds, and coagulation can reduce organic matter and pathogens but are not effective in removing dissolved inorganic anions. Consequently, effluents often retain high anion concentrations, creating persistent water quality challenges in receiving rivers and streams (Kayira & Wanda, 2021). Since the problem is most visible at the municipal wastewater treatment level, where large volumes of effluent are released, this study focused on municipal wastewater as the target application.

Several advanced technologies exist for removing inorganic anions from wastewater, including ion exchange, reverse osmosis (RO), chemical precipitation, evaporation, electrodialysis and advanced reduction processes. While effective, these methods are costly, energy-intensive, require skilled operators, and often generate secondary wastes such as brine or sludge (Ayach et al., 2024; Al Mehrate et al., 2025). In Malawi, most wastewater treatment plants rely on conventional which do not effectively remove dissolved anions. Only a few pilot or industrial plants use advanced technologies, and these are not widely applied. This highlights the need for affordable, locally available solutions such as baobab shell-derived activated carbon that can target inorganic anions efficiently without high costs or complex operations.

Adsorption, particularly using activated carbon, is widely recognized as an effective, economical, and environmentally friendly method for pollutant removal. Activated carbon has a high surface area, well-developed microporous structure, and reactive surface chemistry, enabling it to adsorb various pollutants efficiently. Despite its effectiveness, commercial activated carbon is expensive and its regeneration is costly, limiting widespread use in resource-constrained settings like Malawi (Pet et al., 2024).

Previous studies on baobab shell–derived activated carbon have reported adsorption efficiencies of 93.2% for heavy metals and 99.5% for methylene blue, indicating its strong potential among low-cost adsorbents (Vunain et al., 2017c; Vunain & Biswick, 2019). This research evaluated its performance in removing inorganic anions, addressing a critical knowledge gap and providing valuable insights into the effectiveness of baobab-derived activated carbon compared to commercial alternatives.

1.2 Problem statement

Water pollution from untreated or inadequately treated domestic wastewater remains a major threat to environmental sustainability and public health in Malawi. Conventional treatment systems do not effectively remove dissolved inorganic anions such as nitrates and sulphates, leading to eutrophication, ecological imbalance, and health risks (Kayira & Wanda, 2021). Although activated carbon is an effective adsorbent, its high-cost limits use in local treatment systems. This creates a need for affordable and sustainable alternatives. Therefore, this study investigates baobab shell–derived activated carbon as a low-cost, efficient adsorbent for improving the removal of inorganic anions from domestic wastewater.

1.3 Study objectives

Main objective

To evaluate the efficiency of baobab shell derived activated carbon in removing inorganic anions from domestic wastewater

Specific objectives

1. To characterize the physical and chemical properties of activated carbon produced from baobab shells.

2. To determine the micropore structure and surface characteristics of the baobab shell activated carbon.
3. To assess the adsorption performance of baobab shell derived activated carbon in removing inorganic anions from domestic wastewater.

1.4 Research questions

1. What are the key physical and chemical properties of activated carbon produced from baobab shells?
2. What is the micropore structure and surface characteristic of baobab shell-derived activated carbon?
3. How effective is baobab shell-derived activated carbon in clarifying domestic wastewater and adsorbing inorganic anions (nitrate and sulphate)?

1.5 Scientific significance of the study

This study is important as it advances sustainable wastewater treatment and contributes scientifically by:

- **Promoting waste-to-resource innovation:** converting baobab shells, an agricultural byproduct, into a low-cost adsorbent, thus addressing solid waste issues.
- **Enhancing treatment efficiency:** offering an affordable alternative to conventional methods that fail to remove dissolved anions effectively.
- **Contributing to knowledge:** providing data on the structural and adsorption characteristics of baobab-based activated carbon for environmental applications.

Beyond its scientific contributions, the study aligns with several Sustainable Development Goals (SDGs):

- SDG 6: Clean Water and Sanitation – by providing affordable and sustainable wastewater treatment options.
- SDG 3: Good Health and Well-being – by reducing waterborne health risks.
- SDG 12: Responsible Consumption and Production – by recycling agricultural waste into useful products.

CHAPTER 2: LITERATURE REVIEW

2.1 Domestic wastewater and inorganic anions

Wastewater is water contaminated through human activities, containing physical, biological, and chemical pollutants. Domestic wastewater, produced by households and institutions during cooking, bathing, laundry, and sewage disposal, is classified as blackwater (urine and faeces) or greywater (showers, dishwashing, laundry) (Lakshmi & Reddy, 2017; Gray, 2010). While more uniform than industrial or stormwater wastewater, it still poses serious environmental and health risks if untreated.

It contains organic matter, pathogens, nutrients, and dissolved inorganic salts such as nitrates and sulphates. These ions come from household sources: nitrates from urine and nitrogen-rich waste; sulphates from excreta and cleaning products. Unlike organic matter, they are colourless, odourless, and chemically stable, making them hard to detect but impactful on water quality.

High levels of these anions affect both health and the environment. Nitrates can cause eutrophication and methemoglobinemia (Mihayo et al., 2022). Sulphates may lead to pipe scaling, Odors, and gastrointestinal issues. Conventional treatment systems do not remove inorganic anions effectively, making them persistent challenges, especially in developing countries.

Water scarcity and wastewater reuse for irrigation

Water scarcity, exacerbated by population growth, climate change, and droughts, threatens agriculture in Malawi. Wastewater reuse offers a reliable water source for irrigation, improving food security and resilience (Jodar-Abellan et al., 2019).

Effluent quality, particularly chlorides and nitrates, determines reuse safety. Chlorides accumulate in crops, causing leaf burn and defoliation, while high nitrates and chlorides in irrigation structures promote algal growth and corrosion (Ayers & Westcot, 2024; Hashem & Qi, 2021). Efficient management of these anions can make wastewater a safe irrigation source.

2.2 Limitations of conventional wastewater treatment

Globally, conventional wastewater treatment systems such as stabilization ponds, sedimentation tanks, and activated sludge processes are designed mainly to remove organic matter and suspended solids, but they are often ineffective at eliminating dissolved inorganic anions like chlorides, sulphates, nitrates, and phosphates. Kumar et al. (2023) reported that chloride ions persist through conventional treatment unless advanced technologies, such as ion exchange or reverse osmosis, are used. However, these methods are costly, energy-intensive, and require specialized expertise, making them impractical for low-resource or rural settings.

In Malawi, the limitations of conventional treatment are evident. Ngoma et al. (2020) found that the decentralized system at Mzuzu University reduced BOD and COD effectively, but nitrate and phosphate levels remained high. Similarly, Kayira and Wanda (2021) reported low removal efficiencies at Mzuzu Central Hospital's oxidation ponds, with TDS, nitrates, and phosphates inadequately treated.

Southern Malawi shows similar trends. At Manase WWTP, nitrate concentrations reached 39 mg/L in the dry season and 75 mg/L in the rainy season, while phosphates were 2.0 mg/L and 1.4 mg/L, respectively. Soche WWTP recorded nitrate levels of 37 mg/L (dry) and 445 mg/L (rainy), exceeding Malawi Bureau of Standards (MBS) and WHO limits (Malikula et al., 2022).

In Lilongwe, Kauma Wastewater Treatment Plant relies on stabilization ponds where nitrogen and phosphorus persist due to insufficient nutrient removal. BOD_5 reductions were only 52% in anaerobic ponds and 47% in facultative ponds, with effluent COD and TSS often above national and WHO limits (Ravina et al., 2021; Mdolo, 2017). In Rumphi, Livingstonia Wastewater Stabilization Ponds discharge effluents with elevated BOD, E. coli, phosphates, and suspended solids, significantly degrading the Mpopi Stream (Jere, 2024). Financial, infrastructural, and technological constraints further worsen inorganic pollutant removal (Mumba et al., 2021).

These findings highlight the urgent need for alternative, cost-effective treatment solutions, such as locally available adsorbents like baobab shell–derived activated carbon, to address persistent nutrient pollution.

Table 1: Mean influent and effluent of inorganic anions and removal efficiencies from selected WWTP in Malawi

Inorganic anions	Mean influent(mg/l)	Mean effluent(mg/l)	Removal efficiency(%)	Study area	reference
NO^-_3 TP(total phosphorous)	13.00 1.87	12.00 1.67	7.69 10.87	Rumphi WWTP	(Jere, 2024)
PO^{3-}_4 NO^-_3 Cl^- SO^{2-}_4	67.7 27.8 32.3 0	50.5 9.8 34.0 0	25.4 64.7 -5.3	Chancellor collage WWTP	(Lundgren, 2013)
PO^{3-}_4 NO^-_3 Cl^- SO^{2-}_4	163.4 36.1 129.5 0.3	21.3 24.5 26.6 0.2	86.9 32.13 79.5 33.3	Zomba WWTP	(Lundgren, 2013)
Dry season NO^-_3 Cl^-	 44.8 34.8	 152.9 33.4	 -241 4.0	Blantyre WWTP	Chipofya et al. 2010
Wet season NO^-_3 Cl^-	 84.47 36.9	 32.37 36.2	 61.6 1.9	Blantyre WWTP	Chipofya et al. 2010

2.3 Adsorption and activated carbon

2.3.1 Adsorption

Adsorption is a physical technique where solid materials(adsorbents) are used to remove contaminants from liquids or gases by binding them onto the adsorbent surface through mechanisms such as physisorption, chemisorption and electrostatic attraction(Soffian et al.,

2022) . the method is widely recognized for being effective, versatile and environmentally friendly. Compared to other water treatment techniques, adsorption is economical, requires minimal energy input and is relatively simple to design and operate(Fröhlich et al., 2018) . These attributes make it an attractive option for addressing dissolved pollutants such as inorganic anions, which are inadequately removed by convectional wastewater treatment processes.

2.3.1.1 Competitive adsorption and strategies to manage it

Domestic wastewater contains multiple ions that compete for adsorption sites, a phenomenon called competitive adsorption, which can reduce removal efficiency compared to single-ion systems. Phosphate, for example, often outcompetes nitrate and sulphate due to higher adsorption affinity (Constantino et al., 2017; Villabona-Ortíz et al., 2022a). To address this, batch experiments with multicomponent solutions are conducted to simulate real wastewater, while optimizing pH, adsorbent dose, and contact time enhances target ion uptake (Villabona-Ortíz et al., 2022b; Wang et al., 2018; Vunain et al., 2017c). Surface modifications, such as acid activation or amine functionalization, further improve selectivity by adding functional groups that preferentially bind target anions (Constantino et al., 2017; Shi et al., 2022). This study will manage competitive adsorption through controlled batch experiments with real secondary effluent, optimized operational conditions, surface-activated BFS-AC, and adsorption modelling, ensuring realistic results for effective effluent polishing and safe water reuse.

2.3.2 Activated carbon: production methods, activating agents, methods advantages and disadvantages

Activated carbon is a widely used adsorbent due to its high surface area, large pore volume, and microporous structure, which provide excellent adsorption capacity(Vunain et al., 2019a). It effectively removes various pollutants such as organic compounds, heavy metals, dyes, and salts, making it useful in wastewater treatment, decolorization, catalysis, and medical applications (Hossain et al., n.d.).Its performance depends on the raw material, preparation method, and surface chemistry, which influence its interaction with target pollutants (Nedjai, Alkhatib, et al., 2021). However, commercial activated carbon is costly and mainly produced from non-renewable materials like coal, peat, and petroleum residues, raising economic and environmental concerns (Reza et al., 2020;

Njewa & Shikuku, 2023). To address these issues, recent studies have focused on producing low-cost activated carbon from agricultural wastes such as rice husks, maize cobs, coconut shells, sugarcane bagasse, banana peels, and baobab shells, which show promising adsorption performance (Njewa & Shikuku, 2023; Oloriegbe et al., 2022). This approach reduces reliance on non-renewable resources and promotes waste valorisation, enhancing sustainable solid waste and water management (Kodzwa et al., 2015).

Production methods (procedure)

Activated carbon (AC) can be produced through physical or chemical activation, with chemical activation preferred for its lower temperature requirements, higher carbon yield, larger surface area, and reduced energy costs (Nedjai et al., n.d.).

For baobab fruit shells (BFS), two methods are common: single-step chemical activation and two-step activation.

In **single-step activation**, raw BFS are impregnated with agents like H_3PO_4, KOH, or $ZnCl_2$ and then heated once, allowing carbonisation and activation to occur simultaneously. This process yields highly porous carbon with well-developed micro- and mesopores, ideal for water treatment due to its efficiency and lower energy demand (Ndiaye et al., 2022a; Nedjai et al., n.d., 2022; Vunain et al., 2017d, 2019a).

In contrast, the **two-step method** first carbonises BFS into char, followed by either chemical or physical activation using steam or CO_2. Although it provides better process control, it is more energy-intensive and costly but suitable where chemical use must be minimised (Shang et al., 2023a).

Activating Agents: Implications for BFS-AC and Anion Removal

The activating agent strongly influences the pore structure, surface chemistry, yield, and adsorption performance of baobab fruit shell activated carbon (BFS-AC). Phosphoric acid (H_3PO_4) enhances mesopore formation, introduces oxygenated groups, and achieves high yields (≈46–80%) with cost-effectiveness, though thorough washing is needed to remove residual phosphates (Debbache et al., 2024; Vunain et al., 2017a). Potassium hydroxide (KOH) produces highly microporous carbon with very high surface area (>1000 m^2/g) but lower yields and requires extensive washing to remove corrosive residues (Nedjai et al.,

2021). Zinc chloride ($ZnCl_2$) generates good porosity but leaves toxic residues, limiting its use in low-resource contexts (Nedjai et al., 2021). Physical activation using steam or CO_2 avoids chemical waste but is energy-intensive and less feasible for small-scale production. Considering cost, safety, and adsorption efficiency, H_3PO_4 activation is preferred for BFS-AC in water treatment, offering a practical balance of yield and surface properties in resource-limited settings (Vunain et al., 2017; Ndiaye et al., 2022).

2.4 Baobab fruit shell as a sustainable adsorbent

2.4.1 Availability and Socio-Environmental Rationale

Baobab (*Adansonia digitata*) fruit shells (BFS) are carbon-rich lignocellulosic residues produced in large quantities during fruit processing. The baobab tree, common across Malawi's southern, central, and northern regions, supports livelihoods through its food, Fiber, and medicinal uses (Vunain et al., 2017a). However, discarded BFS often contribute to solid waste challenges, especially in rural areas. Converting these residues into activated carbon offers a sustainable solution by valorising waste biomass and reducing environmental impacts (Ndiaye et al., 2022a).

2.4.2 Lignocellulosic composition and implications on AC production

Baobab fruit shells (BFS) are ideal precursors for activated carbon due to their high carbon, low ash, and lignocellulosic composition (Kodzwa et al., 2015). During thermal conversion, cellulose and hemicellulose form pores, while lignin enhances char stability and yield (Soonmin et al., n.d.). The resulting activated carbon has a high surface area (>1000 m^2/g) and strong adsorption capacity for various pollutants (Nedjai et al., 2021; Ndiaye et al., 2022a; Vunain et al., 2017a). Their abundance and low cost make BFS a sustainable and efficient precursor for activated carbon production in Malawi.

2.4.3 Empirical performance and efficiencies

Studies in Algeria, Zimbabwe, and Senegal show that baobab fruit shells (BFS) can be effectively converted into activated carbon with high porosity and adsorption capacity (Kodzwa et al., 2015; Ndiaye et al., 2022b; Nedjai et al., 2021). In Malawi, BFS-derived activated carbon has shown strong potential for removing heavy metals and dyes, achieving up to 93.17% Cu(II) and 99.5% methylene blue removal(Vunain et al., 2017a, 2019a). Similar success in Tanzania, with nitrate removal of 88.95%, further supports its

versatility (Mihayo et al., 2022). However, limited research has examined its ability to remove inorganic anions like chlorides, nitrates, and sulphates, highlighting the need for local studies under Malawian conditions.

2.4.4 Yield considerations

Yield is a key factor in selecting a precursor for activated carbon, as it affects production cost. Baobab fruit shells (BFS) produce high yields, especially when chemically activated with phosphoric acid (45–80%), depending on activation conditions (Ndiaye et al., 2022a; Nedjai et al., 2021; Vunain & Biswick, 2019b). In contrast, KOH activation gives lower yields (30–50%) despite high surface areas (Mohammed et al., 2019). Compared to other agricultural residues like rice husks, banana peels, and coconut shells, BFS offers competitive or superior yields with comparable surface area (Kodzwa et al., 2015). High yield reduces material needs and overall treatment costs, making BFS-AC economically attractive for large-scale wastewater treatment in resource-limited settings like Malawi.

2.5 Research Gap

Baobab fruit shells (BFS) are abundant, renewable, and can be converted into activated carbon with high porosity and strong adsorption capacity. Global studies show BFS-derived activated carbon effectively removes organic pollutants and dyes (Kodzwa et al., 2015; Ndiaye et al., 2022; Nedjai et al., 2021), while Malawian research demonstrates successful removal of heavy metals and methylene blue (Vunain et al., 2017; Vunain & Biswick, 2019). However, most studies focus on metals and organics, leaving a gap in understanding its performance for inorganic anions in domestic wastewater a key issue in Malawi, where conventional treatment do not remove these ions effectively. Investigating BFS-derived activated carbon for anion removal is therefore essential to develop affordable, sustainable wastewater treatment strategies that improve water quality and public health.

CHAPTER 3: METHODOLOGY

3.0 Introduction

This chapter will discuss about the study area, research design and methods that were employed for sampling, data collection and analysis in order to achieve the specific objectives. The data for this study was obtained from MUST wastewater treatment plant. Several tasks were undertaken such as in-situ water quality parameter testing and laboratory analysis. Furthermore, the data was analysed using Microsoft Excel.

3.1 Study area

Wastewater samples used in this study were collected from the wastewater treatment plant at Malawi University of Science and Technology (MUST). The treatment plant receives and treats wastewater generated from institutional activities within the university. Effluent wastewater samples were specifically collected after treatment to evaluate the removal of inorganic anions, namely nitrate and sulphate, using raw baobab shell adsorbent and baobab shell activated carbon. The collected samples were transported to the laboratory in clean plastic containers for subsequent analysis and adsorption experiments. Figure 1 shows the map of the MUST campus where the wastewater treatment plant is located.

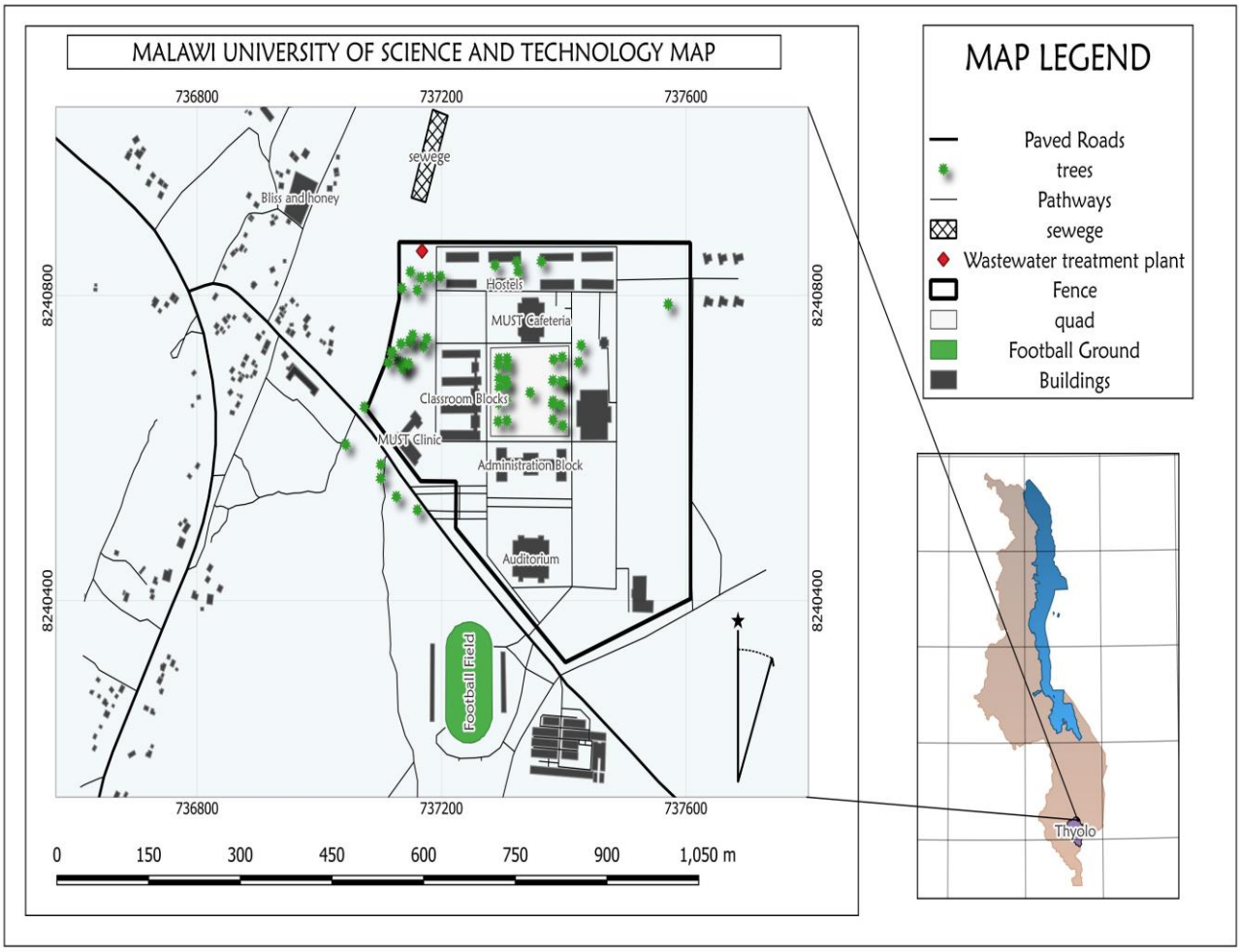


Figure 1: Map of MUST CAMPUS

3.1 Research design

Quantitative true experimental research design was used to conduct this study. This is because it enables objective measurement of adsorption performance under controlled conditions. This approach allows for hypothesis testing and the establishment of clear cause–effect relationships between experimental variables. Batch adsorption experiments were carried out using domestic wastewater, with parameters such as pH, adsorbent dosage and contact time systematically varied to determine their effect on the removal efficiency of nitrates, and sulphates.

3.2 Sampling design

This study used purposive sampling, focusing on effluent (treated) wastewater from the MUST wastewater treatment plant. Samples were collected at selected time intervals to

capture variations in wastewater characteristics throughout the day. Specifically, sampling was conducted in the morning and at midday (lunch time) to account for temporal fluctuations in effluent quality.

Composite representation of the effluent conditions was achieved by considering samples from different times of the day, allowing for the determination of average wastewater characteristics. This approach ensured that the data reflected typical effluent conditions rather than a single-time snapshot.

Purposive sampling was appropriate for this study as it targeted relevant treatment output for wastewater polishing assessment, ensuring that the collected data were suitable for evaluating inorganic anion concentrations and overall treatment performance.

3.3 Materials and methods

3.3.0 Measurement of wastewater parameters

All analyses were conducted by following the Standard Methods for the Examination of Water and Wastewater (APHA, 2017). This was done to ensure accuracy and comparability of results. Physicochemical parameters including temperature, electrical conductivity (EC), and pH were measured on-site immediately after sample collection, as they are highly sensitive to environmental changes. Nitrate and sulphate were determined in the laboratory using standard analytical techniques.

Each sample was clearly labelled with a unique sample ID, date, and time of collection to maintain traceability. Observations of environmental conditions such as rainfall events or unusual discharges during sampling were also documented, as these may influence wastewater quality.

Table 2: Wastewater parameters and methods that were used.

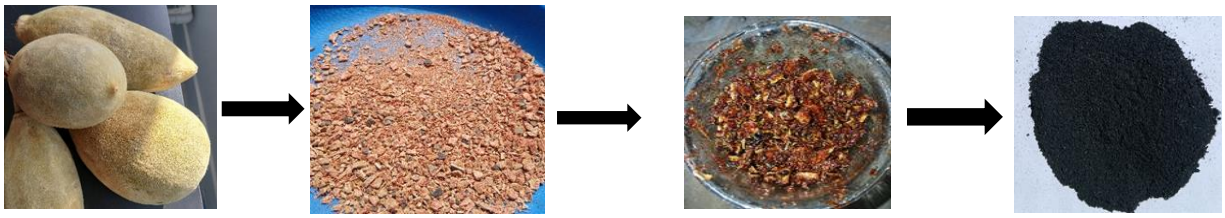
WASTEWATER PARAMETER	METHOD/TECHNIQUE	UNITTS
Temperature	Multi-parameter probe	°C
PH	Multi-parameter probe	-
Electric conductivity	Conductivity meter/ multi-parameter probe	μS/cm
Nitrate	UV-Visible Spectrophotometer	mg/l
Sulphate	UV-Visible Spectrophotometer	mg/l

3.3.1 Production of baobab shell activated carbon

The production procedure for baobab shell activated carbon was adopted from the method described by Vunain et. al (2017). Baobab fruit shells were procured from local markets and community vendors within the Lilongwe District, by selecting only dry and mature shells free from mold or decay. The fruits were broken manually to separate the fruit shells from the ovoid seeds. This was followed by washing with distilled water to remove dirt and surface impurities. Clean shells were sun-dried for 2 days to reduce moisture content, then crushed using a mortar and pestle into pieces of about 2–3 cm. The crushed pieces were sieved to obtain material between 2 and 4 mm in size. Thereafter, the sieved shells were soaked in 85% phosphoric acid (H_3PO_4) at an impregnation ratio of 1:1.75 (char: acid, w/w) for 24 hours at room temperature.

After impregnation, the shells were air-dried at room temperature for 12 hours to remove excess acid. About 100 g of the impregnated shells were placed into pre-weighed glass crucibles followed by carbonization in a muffle furnace at 700°C for 2.5 hours under oxygen-limited conditions. The resulting carbon was ground into a fine powder using a mortar and pestle. Not only that, but also washing of powdered carbon repeatedly with approximately 1 L of deionized water and few drops of 1M NaOH using a Buchner funnel

and flask to remove residual phosphoric acid until filtrate PH reached 6-7 and oven-dried at 105°C for 50 minutes. The dried carbon was sieved through a 106-μm mesh to obtain fine, uniform activated carbon powder and the final baobab shell activated carbon (BFSAC) was stored in airtight containers and labelled appropriately for later use in characterization and adsorption experiments. The preparation stages of baobab shell activated carbon are shown in Figure 2.



(a) (b) (c) (d)

Figure 2: Flow diagram showing the preparation stages of baobab fruit shell activated carbon: (a) raw baobab shells, (b) crushed baobab shells, (c) phosphoric acid impregnated shells, and (d) final activated carbon

3.3.2 Preparation of raw baobab shell adsorbent (RB)

Impurities associated with the baobab shells were removed by washing with distilled water. The cleaned shells were then sun-dried for 2 days to reduce moisture content, followed by oven drying at 80°C until a constant mass was achieved. The dried shells were subsequently crushed and sieved to obtain smaller particle sizes. The prepared (Figure 3) adsorbent was then stored in an airtight container to prevent contamination or any unwanted reactions prior to characterization and adsorption experiments (Ali, Asim, & Khan, 2012).



(a) (b)

Figure 3: Graphic diagram of raw adsorbent preparation, (a) raw baobab fruits and (b) Powdered baobab fruit shells.

3.3.4 Physical and chemical characterisation of BFS-AC

1. Carbon yield

This was performed by Weighing raw dried baobab shell before processing as W_{raw}. Thereafter, weigh dry activated carbon after activation and drying as W_{AC}.

Carbon yield was Calculated as:

$$\text{Yield (\%)} = \frac{W_{\text{AC}}}{W_{\text{raw}}} \times 100$$

2. Moisture content

This was performed by weighing 1g of the sample as (W1), followed by drying in an oven at 105°C for 3 hours. Finally, the sample was cooled in desiccator and final mass was obtained as (W2).

$$\text{Moisture (\%)} = \frac{W1-W2}{W1} \times 100$$

3. Volatile matter

5g of the activated carbon/raw baobab sample was weighed to obtain initial mass. The sample was then placed into a covered crucible to prevent oxygen from entering. The sealed crucible was heated in a muffle furnace at 925 °C for 7 minutes followed by cooling in a desiccator to cool. Finally, the crucible was weighed again to obtain the final mass of the remaining material.

Volatile matter percentage was computed using this formula:

$$\%VM = \frac{\text{Weight of volatile matter}}{\text{Weight of original sample}} \times 100$$

Weight of volatile matter = Initial mass – Final mass

4. Ash content

A mass of 1.0 g of the dried activated carbon sample was accurately weighed and recorded as the initial weight (W_o). The sample was then placed in a clean porcelain crucible and transferred into a preheated muffle furnace set at 1000 °C. The sample was heated for 1 hour to ensure complete combustion of all organic matter.

After heating, the crucible was carefully removed from the furnace and placed in a desiccator to cool to room temperature. Once cooled, the crucible and its contest was weighed to obtain the final weight (W).

Calculated the percentage ash content using:

$$W_0 - W = W_{ash}$$

$$\%\text{Ash Content} = \frac{W_{\text{ash}}}{W_0} \times 100$$

5. pH at point of zero charge

The pH at the point of zero charge (pH_pzc) was determined using the pH drift method. A series of 0.01 M NaCl solutions (100 mL each) were prepared and their initial pH values adjusted to 2, 3, 4, 5, 6, 8 and 10 using 0.1M HCl or 0.1M NaOH.

To each solution, 0.1 g of activated carbon/raw adsorbent was added. The suspensions were then agitated for 24 hours at room temperature to allow equilibrium to be reached. After equilibration, the final pH of each solution was measured.

Plot ΔpH (final − initial) vs initial pH

pHpzc is point where ΔpH = 0

3.3.5 Micropore and surface characteristics

1. Pore volume and porosity

The pore volume of the activated carbon was determined using the saturation method as described by Mihayo et al. (2022), with slight modifications. 1g of activated carbon/raw

baobab was placed in a 10 mL measuring cylinder and the initial volume of the dry sample was recorded as the particle volume.

The sample was then mixed with 20 mL of distilled water and heated for 5 minutes to enhance saturation of the pore spaces. After heating, the sample was removed, excess water was drained, and it was left to dry at room temperature for 24 hours. The final weight was then recorded.

Pore volume was calculated as the amount of water absorbed:

$$\text{Pore volume (mL)} = \text{Final weight} - \text{Initial weight}$$

Using water density = 1 g/mL, calculated porosity using:

$$\text{Porosity} = \text{Pore volume} / \text{Initial volume of sample}$$

2. Iodine number (micropore content)

The iodine number of the activated carbon was determined to evaluate its micropore content using a modified ASTM D4607 procedure (ASTM International, 2021). A standardized 0.05 M iodine solution was used; therefore, no preparation or standardization of the iodine solution was carried out.

For the adsorption experiment, 0.5 g of the activated carbon sample was accurately weighed and transferred into a 250mL conical flask. A volume of 10 mL of 5% (v/v) hydrochloric acid (HCl) was added, and the mixture was gently heated on a hotplate for approximately 30 seconds to ensure complete wetting and proper mixing of the carbon.

Subsequently, 100 mL of the iodine standard solution was added to the flask. The mixture was then agitated for 60 minutes to allow adsorption of iodine onto the activated carbon. After the contact period, the suspension was filtered using Whatman filter paper to obtain a clear filtrate.

A 20 mL aliquot of the filtrate was then titrated with 0.1N sodium thiosulfate solution using starch as an indicator. The endpoint was identified by a colour change from blue to colourless, indicating that all iodine had reacted. The volume of sodium thiosulfate used was recorded as S (mL).

A blank titration was carried out by titrating 20 mL of the iodine solution (without activated carbon) under the same conditions. The volume of sodium thiosulfate used for the blank was recorded as B (mL).

The chemical reaction is as follows:

$I_2 + 2S_2O_3^{2-} = 2I^- + S_4O_6$

Where:

I_2 = iodine

$2S_2O_3^{2-}$ = thiosulphate

the amount of iodine adsorbed was calculated using:

$$\text{Iodine number (mg/g)} = \frac{(B - S) * N * 253.81 * Vtotal}{M * Valiquot * 2}$$

Where:

B = volume of thiosulfate used for the blank (mL)

S = volume of thiosulfate used for the sample (mL)

N = normality of sodium thiosulfate (mol/l)

M = mass of activated carbon (g)

253.81 = molecular weight of iodine (I_2), (g/mol)

V_{total} = total iodine solution (ml)

$V_{aliquot}$ =portion of iodine solution titrated (ml)

2= stoichiometric factor (from the reaction)

3.3.6 Batch adsorption experiment procedure (pH, dose, and contact time)

General Preparation

A composite wastewater effluent sample was collected from MUST wastewater treatment plant at selected time intervals to account for diurnal variations in wastewater characteristics. Sampling was conducted in the early morning (06:00–07:00 hours) and at midday (12:00 hours). The collected samples were then combined and thoroughly mixed to obtain a homogeneous bulk sample for the batch experiments.

On-site measurements of pH and electrical conductivity (EC) were conducted immediately after sample collection to capture in-situ conditions. Upon arrival at the laboratory, physicochemical parameters including pH and EC were measured.

The initial concentrations (C_0) of target inorganic anions, specifically nitrate and sulphate, were determined using standard analytical methods prior to the adsorption experiments. All instruments used in this study were calibrated prior to experimental work to ensure accuracy and reliability of measurements. All batch experimental samples were subsequently prepared from this homogenized bulk wastewater to ensure consistent initial conditions across all experiments.

Effect of pH on adsorption

Batch experiments were conducted to evaluate the effect of pH (2, 4, 6, 7, and 8) on anion removal. A volume of 100 mL of wastewater was added into 500 mL beakers, and the pH was adjusted using 0.1 M Hydrochloric acid or 0.1 M Sodium hydroxide.

Activated carbon/raw adsorbent (0.1 g) was added to each flask, and the mixtures were agitated at 150 rpm for 60 minutes. The samples were then filtered, and the final concentrations (C_e) of nitrate (NO_3^-) and sulphate (SO_4^{2-}) were determined. The pH with the highest removal efficiency was selected as the best pH. Figures 4 and 5 illustrate the batch experimental setups for the evaluation of pH effect on anion removal using raw baobab shell adsorbent and activated carbon, respectively.

The removal efficiency was calculated using:

$$\text{Removal } \% = (C_o - C_e)/ C_o * 100 \quad \text{..... equation 3.1}$$

Where:

C_o = initial concentration

C_e = final concentration

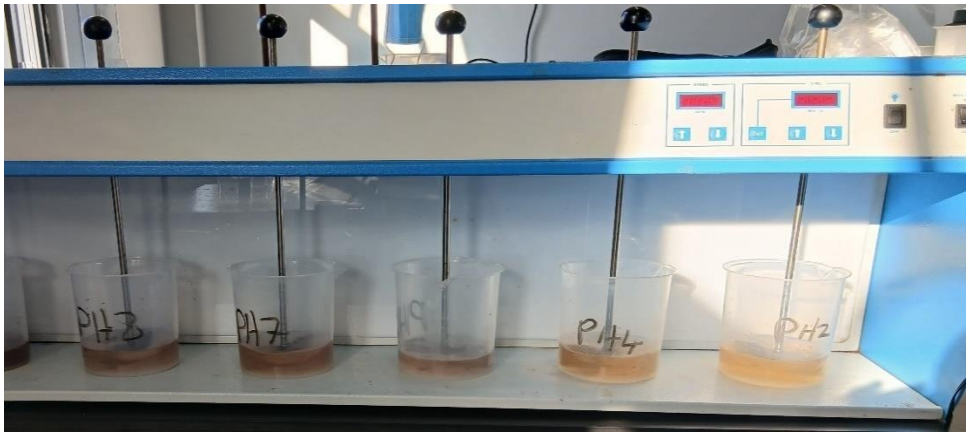


Figure 4: batch experiment setup for evaluation of pH effect on anion removal using RB



Figure 5: batch experiment setup for evaluation of pH effect on anion removal using BFS-AC

Effect of Adsorbent Dose

Batch experiments were conducted using the best pH to evaluate the effect of adsorbent dose (1–5 g). A volume of 100 mL of wastewater (adjusted to optimal pH) was transferred into beakers, and varying masses of activated carbon were added. The mixtures were agitated at 150 rpm for 60 minutes, followed by filtration to separate the adsorbent. The final concentrations (C_e) of the target anions were determined. Removal efficiency was calculated using Equation (3.1), and the dose corresponding to the highest removal was selected as the optimum adsorbent dosage.

Contact Time

Batch experiments were conducted at best pH and adsorbent dose to evaluate the effect of contact time (30–180 minutes). A volume of 100 mL of wastewater was transferred into beakers, and the optimum mass of activated carbon was added. The samples were agitated at 150 rpm, and beakers were withdrawn at predetermined time intervals (30, 60, 90, 120, 150, and 180 minutes). The mixtures were immediately filtered, and the final concentrations (C_e) of the target anions were determined.

3.6 Data analysis

Descriptive statistics were used to summarize wastewater characteristics and to calculate removal efficiencies of inorganic anions. Analysis of variance (ANOVA) was applied to evaluate if differences in treatments were statistically significant, while Pearson correlation analysis was used to assess the relationships between pH, adsorbent dose, contact time, and adsorption performance. Pearson correlation was appropriate because the data were continuous and assumed to have a linear relationship between the variables.

Adsorption isotherms (Langmuir and Freundlich) and kinetic models (pseudo-first-order and pseudo-second-order) were applied to evaluate adsorption capacity and mechanisms. Model fit and accuracy were assessed using the coefficient of determination (R^2) and error functions. All analyses were performed using Microsoft Excel, and results are presented in tables and graphs.

3.8 Study limitations

Due to instrumentation constraints, activated carbon characterisation was conducted using alternative and relatively time-consuming methods. This resulted in slower data generation compared to studies that employ advanced analytical equipment such as SEM, BET surface area analyzers, and other automated instruments. However, standard procedures were followed to ensure the reliability and validity of the results obtained.

CHAPTER 4: RESULTS AND DISCUSSION

4.0 Introduction

This chapter presents and discusses the results of the production, characterization and adsorption performance of the prepared activated carbon and raw adsorbent (raw baobab). The physicochemical properties and surface characteristics of the activated carbon and raw baobab are presented, followed by batch experiment results, under varying conditions of pH, adsorbent dosage, and contact time. Tables and graphs are used to present the obtained results.

5.1 Production and physicochemical characterisation of BFS-AC

5.1.1 Carbon yield of activated carbon

The activated carbon was produced from baobab fruit shells (BFS) through single-step chemical activation using phosphoric acid (H_3PO_4) at an impregnation ratio of 1:1.75 (char: acid, w/w), followed by carbonisation, washing with distilled water, and neutralisation with dilute 1 M NaOH. The production parameters and yield are presented in Table 3.

Table 3: The production and yield parameters

PARAMETER	VALUE	NOTES
Initial biomass	270.8g	Raw biomass
Mass after carbonization and activation	190.4g	Post H3PO4 activation
Carbon yield	70.3%	
Final Ph after washing	7.05	Near-neutral; residuals removed

The activated carbon produced had a final weight of 190.4g from an initial biomass weight of 270.8g. The total yield of carbon produced was 70.3%. Carbon yield is defined by Vunain et al. (2017) as the amount of the original precursor material that remains after pyrolysis and activation processes. The relatively high carbon yield is attributed to the activation ratio of carbon char to acid (w/w) being appropriately selected at 1:1.75, thereby maximizing the carbon content throughout the carbonization process and

encouraging the formation of carbon structure. The activated carbon was shown to have near-neutral pH (7.05) following cold water wash with distilled water and 1M sodium hydroxide this represents a successful wash out of any residual activating agents and process contaminants. An adsorbent surface that is near-neutral pH has implications for potential use as an adsorption medium as there will be no interference by residual activating constituents. The findings support those of Vunain et al. (2017) 78% yield for carbon produced under identical activation conditions. The difference in yield can be attributed to differences in raw material properties and experimental conditions. This yield is consistent with the range of 45–80% reported by Ndiaye et al. (2022) and is slightly below the 78% reported by Vunain et al. (2017) under similar H_3PO_4 activation conditions. The minor difference may be attributed to variations in raw material composition and carbonization conditions. Compared to KOH-activated BFS-AC, which typically yields 30–50% (Nedjai et al., 2021), the H_3PO_4 approach demonstrates clear advantages in carbon retention, reinforcing its suitability for low-resource production settings such as Malawi.

5.1.2 Moisture content

Moisture in activated carbon exists as free water physically adsorbed within the pore network and as bound water associated with surface functional groups through hydrogen bonding

Activated carbon moisture content normally originate from two sources; the first one is from free water which is located in the pore area of thin carbon, and from bound water which is attached to the surface of thin carbon via hydrogen bonds or chemical bonds (Zeng, Loi, Shi, & Liu, 2024). High moisture content is particularly unfavourable because these water molecules occupy the same surface sites that are needed for target anion uptake: they compete directly with NO_3^- and SO_4^{2-} for electrostatic and coordination binding sites, and can form hydration shells around active functional groups that hinder anion approach (Bhatnagar, Hogland, Marques, & Sillanpaa, 2013). The results of moisture content are presented in 4.

Table 4: moisture content of BFS-AC

Trial	Crucible weight (g)	Initial mass of AC(g)	Final mass (crucible + AC)	Final AC mass (g)	Moisture weight	Moisture content%
1	16.653	1	17.638	0.985	0.015	1.5
2	8.535	1	9.519	0.984	0.016	1.6
3	8.624	1	9.613	0.989	0.011	1.1
AVERAGE						1.4

A mean moisture content of 1.4% therefore confirms that the BFS-AC surface is predominantly accessible, with minimal water competition at the adsorption interface. Mihayo et al. (2022) and Vunain et al. (2019) Mihayo et al. (2022) and Vunain et al. (2019) reported BFS-AC to have moisture values of approximately 3.7% and 1.58%, respectively and the moisture value obtained in this study (1.4%) is less than that from either previous study because of the longer period of drying to remove residual interstitial moisture that shorter drying periods would leave in the sample.

5.1.3 Volatile content

In order to determine volatile matter content for BFS-AC, three trials were conducted. The sample was heated in a muffle furnace under a control conditions. The average value of 23.01% was calculated as shown in table 5.

Table 5: Volatile matter of BFS-AC

Crucible weight(g)	Initial mass of AC (g)	Final mass (g)	AC final mass (g)	VM weight (g)	Volatile matter %
44.208	5.0099	47.9988	3.7905	1.2195	24.34
40.807	5.0003	44.6520	3.845	1.1553	23.10
45.304	5.0141	49.2360	3.932	1.0821	21.58
Average					23.01

According to Pereira et. al (2011), volatile matter indicates presence of labile organic fractions in activated carbon. These organic fractions are the ones that have not been transformed into stable aromatic carbon structure during the process of carbonization. During carbonization process, these compounds undergo dehydration, decarboxylation, and condensation reactions driven by presence of activating agent (H3PO4). Therefore, the volatile organic by-products are released as gases (CO_2, CO, H_2O vapor, and hydrocarbon fragments), and the resulting voids form the micropore and mesopore network of the activated carbon.

This means that, the greater the percentage of residual volatile matter, the higher the concentration of labile organic matter in the carbon matrix as a result of incomplete combustion and these occupy pore spaces resulting in blockage of adsorption sites.

The moderate value of 23.01% for activated biomass indicate that carbonization and chemical activation of baobab fruit shells resulted in high quality activated carbon for wastewater treatment via adsorption. Despite having moderate value of 23.01% which also reflects a graphitized and porous structures for BFS-AC, it is falling outside the range of 20–22% reported by Dav et al. (2012) for comparable agricultural-waste carbons, but still suggesting similar carbonization conditions due the closeness of these values.

Mihayo et al. (2022) revealed a minimum value of 15%, which can be attributed to more thorough volatilization caused by a higher activation temperature. However, through non-electrostatic mechanisms, more vigorous volatilization can concurrently lower the density of oxygenated surface functional groups that support anion uptake. The lower value of 1.8% reported by Vunain et al. (2019) reflects a fundamentally different carbonization methodology at higher temperature (>700°C), which produces a more fully graphitized carbon with lower functional group density, a gap that the present study addresses by demonstrating that intermediate carbonization conditions maintain a higher density of reactive surface groups relevant for inorganic anion adsorption at neutral pH.

4.1.4 Ash content

Ash content was determined by complete combustion of both BFS-AC samples in a muffle furnace. The mean ash content for BFS-AC was 9.27%, as presented in Table 6.

Table 6: Ash content of BFS-AC

Trial	Crucible (g)	Initial AC (g)	Final mass (g)	Final AC (g)	Ash (g)	Ash (%)
1	23.964	1.021	24.877	0.913	0.108	10.55
2	20.056	1.004	20.977	0.921	0.083	8.22
3	25.562	1.000	26.472	0.910	0.090	9.03
Average						9.27

Ash in activated carbon is an indicator of non-combustible inorganic minerals which are primarily silicates, phosphates, carbonates, and metal oxide originating from the mineral content of the precursor biomass and from residual activating agent that was not fully removed during washing (Izabella, kamil, Piotr, & Jorg, 2025).

When present in higher concentrations, these mineral deposits have two disastrous effects on adsorption performance. Firstly, they physically cause blockage of micropore entrances, reducing the accessible internal surface area and pore volume for anion diffusion (Zhu et al., 2024). Not only that, but also introducing competitive adsorption effects by metal oxides that interfere with the anion removal selectivity of the carbon.

Furthermore, alkaline ash components (calcium and magnesium carbonates) can locally raise the pH at the carbon surface, shifting the surface chemistry away from the pH_pzc towards conditions that are less favourable for anion adsorption via electrostatic attraction (Zha et. al, 2015).

The mean ash content of 9.27% obtained in this study is substantially higher than the 1.58% reported by Vunain et al. (2017) and the 1.6% reported by Langama et al. (2023). This gap is chemically significant and is attributed by the factors like washing protocol employed where by distilled water washing with 1 M NaOH neutralization may have been insufficient to remove silicate and phosphate mineral residues that are only soluble under more acidic or prolonged washing conditions. The studies by Vunain et al. (2017) and Langama et al. (2023), which achieved lower ash contents, employed either acid-wash post-treatment or extended sequential washing steps not used in the present work.

5.1.4 pH at point of zero charge

The pH at the point of zero charge (pH_pzc) is a critical surface chemical property that determines the net charge of the adsorbent surface under different solution pH conditions (Sen et.al, 2026). The pH_pzc was determined by plotting the initial solution pH against the change in pH (ΔpH); the pH_pzc corresponds to the point where ΔpH = 0.

The pH_pzc of the prepared BFS-AC was found to be 4.01. This indicates that at pH values below 4.01, the BFS-AC surface carries a net positive charge due to protonation of surface functional groups. Conversely, at pH values above 4.01, surface deprotonation results in a net negative charge. This property directly governs electrostatic interactions between the adsorbent and charged ionic species in solution, and its determination is essential for predicting and interpreting the pH-dependent behavior of anion adsorption, as discussed in Section 4.4.2.1.

The pH_pzc value of 4.01 obtained in this study is consistent with values reported for H_3PO_4-activated carbons in previous studies, confirming that phosphoric acid activation introduces acidic oxygen-containing functional groups, such as carboxyl, phosphate, and phenolic groups, which lower the pH_pzc below neutral conditions. Similar findings were reported by Langama et.al (2023), where phosphoric acid-activated carbon exhibited a pH_pzc of 4.4. The close similarity between the reported pH_pzc value of 4.4 and the 4.01 obtained in the present study suggests that phosphoric acid activation consistently produces acidic surface characteristics regardless of biomass source. This acidic surface character has important implications for anion removal. Although electrostatic attraction of negatively charged anions such as NO_3^- and SO_4^{2-} is thermodynamically favoured mainly at solution pH values below the pH_pzc, the batch adsorption experiments conducted at pH 7 still showed appreciable adsorption capacities. This indicates that, in addition to electrostatic interactions, other adsorption mechanisms such as hydrogen bonding, ligand exchange, pore filling, and chemical complexation may also significantly contribute to anion uptake onto the activated carbon surface.

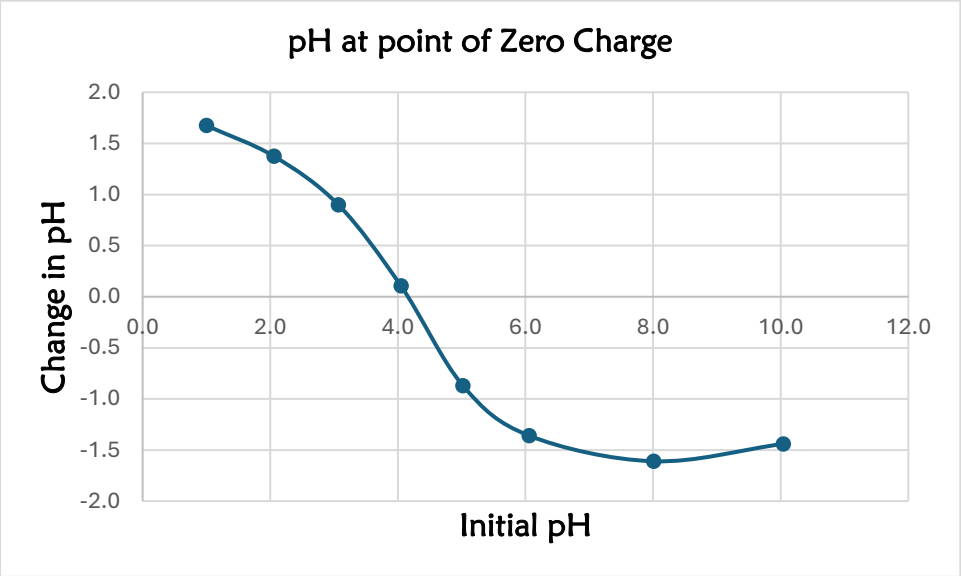


Figure 6: PH at point of zero charge of BFS-AC

5.2 Micropore and surface characteristics

4.2.1 Iodine number

The iodine number of the prepared activated carbon was found to have a mean value of 922.18 mg/g, as presented in Table 7. Iodine number quantifies the number of micropore adsorption sites accessible to iodine molecules (I_2; kinetic diameter ~0.55 nm; molecular weight 253.8 g/mol). Because iodine selectively accesses pores smaller than approximately 2 nm micropores (IUPAC definition), the iodine number directly reflects micropore surface density and active adsorption sites available to inorganic anions of comparable or smaller size. The accepted minimum quality for activated carbon is 500 mg/g (AWWA Standard B600), with values above 900 mg/g indicating high micropore content suitable for small contaminant removal. The mean iodine number of 922.18 mg/g obtained for BFS-AC therefore confirms a well-developed micropore network resulting from the chemical dissolution and dehydration action of H_3PO_4 during carbonization. The value falls slightly below the 1113 mg/g reported by Vunain et al. (2017); this difference is chemically consistent with the higher ash content (9.27% vs. 1.58%) observed in this study, since inorganic mineral deposits can physically block micropore entrances, reducing the fraction of the internal surface accessible to iodine.

Iodine number of 922.18 mg/g surpasses the range of 900–950 mg/g reported for KOH-activated carbons from comparable agricultural feedstocks (Nedjai et al., 2021),

confirming that H_3PO_4 activation is more effective than KOH for generating high micropore density from BFS under the conditions of this study.

Table 7: Iodine number of BFS-AC

Sample	sample volume (ml)	initial V of T(ml)	final V of T	T used (ml)	iodine number (mg/g)
Blank	20	0	17.1	17.1	0.00
1	20	25.5	35.6	10.1	888.34
2	20	0	9.6	9.6	951.79
3	20	9.6	19.4	9.8	926.41
Average					**922.18**

4.2.2 Pore volume and porosity

Pore volume and porosity are key structural parameters that determine the total adsorptive capacity of an activated carbon. In this study, pore volume and porosity were estimated using the saturation method. The results are presented in Table 8

Table 8: pore volume and porosity of BFS-AC

AC initial mass (g)	AC initial volume(ml)	final weight (g)	water adsorbed (g)	pore volume (Cm^3)	particle volume (ml)	porosity %
1	2.5	1.4	0.4	0.4	2.5	16.00
1	2.2	1.6	0.6	0.6	2.2	27.27
1	2.6	1.5	0.5	0.5	2.6	19.23
AVERAGE			0.5	0.5	2.4	20.83

Pore volume refers to the total internal void space within the activated carbon, while porosity represents the fraction of the material occupied by these pores (Phothong,

Tangsanthitkulcga, & Lawtae, 2021). These properties arise from the removal of volatile components and the action of activating agent during carbonization, which create a network of micro and mesopores within the carbon structure (Khamkeaw et. al, 2020). These parameters are critical because ions such as nitrate and sulphate exist in hydrated forms, requiring sufficient pore spaces and connectivity to access adsorption sites. Higher pore volume and porosity enhance adsorption and by improving both capacity and mass transfer while limited pore development can restrict ion diffusion and reduce overall removal efficiencies.

4.3 Validation of activation: performance comparison with raw baobab shell precursor

To confirm that the adsorption performance of BFS-AC is attributable to the chemical activation process rather than to the intrinsic properties of the raw baobab fruit shell (BFS) precursor, a control experiment was conducted in which the un-activated raw biomass was characterized and subjected to the same batch adsorption experiments under identical conditions. This approach provides direct experimental validation of the value added by activating agent (H_3PO_4) and substantiates the claim that the prepared BFS-AC is a genuinely activated carbon whose performance is a product of the activation process.

Physicochemical properties: Raw BFS vs BFS-AC

The physicochemical properties of the raw BFS and the prepared BFS-AC are compared in Table 9. The differences between the two materials yield a significance impact confirming the transformative effect of chemical activation.

Table 9: Comparison of physicochemical properties for Raw BFS and BFS-AC

Property	Raw BFS	BFS-AC
Moisture Content (%)	18.80	1.40
Volatile Matter (%)	56.17	23.01
Iodine Number (mg/g)	122	922.18
Pore Volume (cm^3/g)	0.12	0.50
Porosity (%)	13.00	20.83
PHpzc	6.98	4.01

The data in Table 9, reveal the profound impact of H_3PO_4 activation on every physicochemical parameter measured. Moisture content reduced from 18.80% in raw BFS to 1.40% in BFS-AC indicating a reduction of over 92%. This reflect the removal of physically adsorbed water and bound hydroxyl groups during high-temperature carbonization, and confirming that the vast majority of the BFS-AC surface is dry and accessible for anion uptake. Volatile matter decreased from 57.96% to 23.01%, indicating that the activation step drove extensive pyrolytic volatilization of labile organic fractions, releasing gaseous decomposition products that generated the pore network.

The most reliable indicator of activation quality is the iodine number which increased from 122 mg/g in raw BFS to 922.18 mg/g in BFS-AC. The raw biomass iodine number of 122 mg/g falls well below the 500 mg/g quality threshold (AWWA Standard B600), confirming that the un-activated precursor has negligible micropore content and is unsuitable as an adsorbent. The BFS-AC value of 922.18 mg/g, by contrast, greatly exceeds this threshold, confirming a high-grade activated carbon. Pore volume increased from 0.12 cm^3/g to 0.50 cm^3/g and porosity increased from 13% to 20.83%, both consistent with the creation of an extensive internal pore network during activation. Finally, the pHpzc shifted from 6.98 in raw BFS to 4.01 in BFS-AC, reflecting the introduction of acidic oxygenated functional groups such as carboxyl, hydroxyl, and phosphate groups generated by phosphoric acid (activating agent) which are absent from the un-activated precursor. These results collectively confirm that the BFS-AC produced in this study is a genuinely activated carbon whose structural and chemical properties are entirely a product of the activation process rather than the raw precursor material.

Batch Adsorption Performance: Raw BFS vs BFS-AC

Both adsorbents, the raw BFS and BFS-AC were subjected to identical batch adsorption experiments (effect of pH, dosage and contact time) using the same operating experimental conditions. The comparative removal efficiencies based on the best pH, dosage and contact time are summarized in Table 10 for nitrate and Table 11 for sulphate.

Table 10: Nitrate removal efficiency for Raw BFS vs BFS-AC (effect of pH, dosage, and contact time)

Condition	Variable	Raw BFS Removal efficiency (%)	BFS-AC Removal Efficiency (%)
pH effect	pH 2 (max)	45.60	80.88
Dosage effect	2 g(max)	36.44	89.22
Contact time effect	90 min (max)	39.80	90.45

Table 11: Sulphate removal efficiency for Raw BFS vs BFS-AC (effect of pH, dosage, and contact time)

Condition	Variables	Raw BFS Removal efficiency (%)	BFS-AC Removal Efficiency (%)
pH effect	pH 7 (max)	10.92	40.40
Dosage effect	2 g(max)	29.41	75.85
Contact time effect	90 min (max)	34.03	88.14

The batch adsorption results confirm, in quantitative terms, the superiority of BFS-AC over the un-activated raw precursor across every experimental condition tested. For nitrate removal, BFS-AC outperformed raw BFS at pH 2 (80.88% vs 45.60%), at optimal dosage (89.22% vs 36.44%), and at equilibrium contact time (90.45% vs 39.80%). For sulphate, the performance gap is even more pronounced: BFS-AC achieved a higher removal than raw BFS under pH conditions (40.40% vs 10.92%), at optimal dosage (75.85% vs 29.41%), and at equilibrium contact time (88.14% vs 34.03%). These differences are mechanistically consistent with the physicochemical data in Table 9. The raw BFS has a negligible iodine number (122 mg/g), indicating minimal micropore content and therefore few adsorption sites accessible to inorganic anions. Its high moisture content (18.90%) means that available surface sites are occupied by water molecules, which compete with target anions for adsorption sites and create diffusion barriers within the limited pore structure.

In addition to that, its near-neutral pHpzc of 6.98 compared to 4.01 for BFS-AC means that at working pH values of 2–7, the raw BFS surface carries substantially less positive charge than BFS-AC, reducing electrostatic attraction towards anionic species. By contrast, the BFS-AC benefits from a greater iodine number, greater pore volume, significantly lower moisture content, and a lower pHpzc that creates a more strongly positive surface at acidic pH. Together, these results provide experimental validation that the activation process is responsible for the adsorption performance of BFS-AC, and that the raw baobab shell precursor alone is an insufficient adsorbent for inorganic anion removal from domestic wastewater.

4.4 Wastewater clarification and adsorption performance of BFS-AC

Objective 3 has two components; clarification performance, referring to the overall improvement in wastewater quality parameters following treatment, and adsorption performance, referring specifically to the removal of target inorganic anions (nitrate and sulphate) under optimized batch conditions. Both components are addressed in this section.

4.4.1 Clarification performance of BFS-AC

Clarification performance refers to the general improvement in physicochemical quality of the domestic wastewater following treatment with BFS-AC. The initial and post-treatment wastewater properties are presented in Table 12.

Table 12: Initial and post-treatment physicochemical properties of domestic wastewater

Parameter	Initial (pre-treatment)	Final (post-treatment)	Removal%
Electrical Conductivity (EC)	1087 μS/cm	738 μS/cm	32.1%
Total Dissolved Solids (TDS)	514 mg/L	386 mg/L	24.9%
Odour	Strong / unpleasant	Significantly reduced	

Following treatment with BFS-AC under the batch conditions, significant improvements in wastewater quality were observed. Electrical conductivity (EC) decreased from 1087 to 738 μS/cm, representing a 32.1% reduction. Total dissolved solids (TDS) decreased from

514 to 386 mg/L, a reduction of 24.9%. The unpleasant odor of the raw wastewater was also significantly reduced after treatment.

The reduction in EC reflects a decrease in the concentration of dissolved ionic species in solution, which can directly be attributed to the adsorption of inorganic anions (NO_3^-, SO_4^{2-}) and cations onto the BFS-AC surface. The corresponding decrease in TDS indicates removal of both dissolved inorganic ions and dissolved organic matter through combined adsorption mechanisms including electrostatic attraction, pore filling, and surface complexation. The reduction in odor is attributed to the adsorption of volatile organic compounds and odor-forming compounds, which are commonly present in domestic wastewater and are known to be effectively adsorbed by activated carbons with high micropore content.

These results confirm that BFS-AC functions not only as a selective adsorbent for specific ions but also as a broad-spectrum clarification agent, improving multiple quality parameters simultaneously. This is consistent with the multi-pollutant removal capabilities reported in the literature for H_3PO_4-activated agricultural-waste carbons (Njewa & Shikuku, 2023), and supports the potential of BFS-AC as a practical, low-cost clarification material for domestic wastewater treatment in resource-limited settings.

4.4.2 Adsorption Performance: Effect of pH, Dosage, and Contact Time

Batch adsorption experiments were conducted to evaluate the effects of solution pH, adsorbent dosage (BFS-AC), and contact time on the removal of nitrate and sulphate from domestic wastewater. All experiments were carried out using 100 mL wastewater samples at room temperature with agitation at 150 rpm.

4.4.2.1 Effect of Solution pH on Nitrate and Sulphate Removal

Solution pH governs both the surface charge of the BFS-AC (as determined by the pH_pzc in Section 4.1.4) and the speciation of target anions in solution. The pH was varied from 2 to 8, with all other conditions held constant. The statistical results are presented in Table 13, and the removal efficiencies at each pH level are shown in Figure 7.

Table 13: Statistical analysis of the effect of solution pH on nitrate and sulphate removal

Statistical Measure	Nitrate (NO_3^-)	Sulphate (SO_4^{2-})
ANOVA p-value	0.0000394	8.92×10^{-6}
F-value / F-critical	—	98.68 / 5.32
Correlation coefficient (r)	-0.97	0.23
Optimum Ph	2 (laboratory); 7 (practical)	7
Max. removal at optimum pH	80% (pH 2); ~72% (pH 7)	40.4%
Dominant mechanism	Electrostatic attraction	Surface complexation

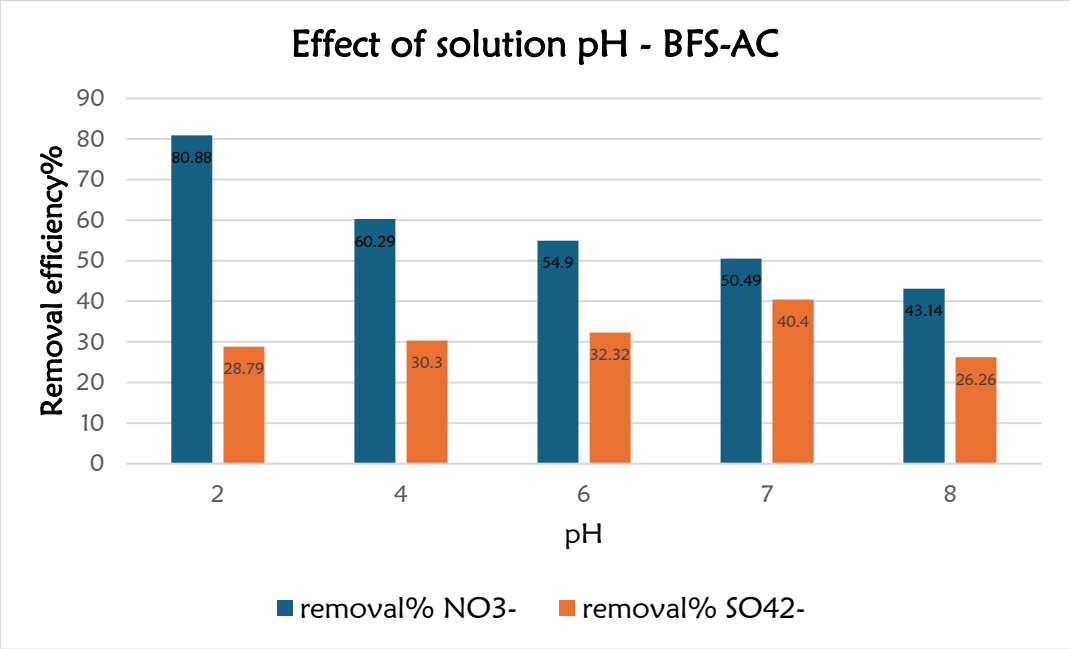


Figure 7: effect of solution pH on removal of NO3- and SO42- by BFS-AC (dosage = 0.1g, time= 60mins, speed=150rpm)

4.4.2.1.1 Nitrate Removal

The highest nitrate removal efficiency of 80% was observed at pH 2, with a progressive and statistically significant decline as pH increased (ANOVA: p = 0.0000394). This behaviour is directly explained by the pH_pzc of 4.01. At pH 2, which is well below the pH_pzc, the BFS-AC surface is strongly positively charged due to protonation of surface

functional groups. This creates a favourable electrostatic attraction between the positively charged surface and the negatively charged nitrate ion (NO_3^-), enhancing adsorption. As pH increases above 4.01, surface deprotonation results in a negatively charged surface, generating electrostatic repulsion towards NO_3^- and increased competition from OH^- ions, both of which reduce adsorption efficiency.

Correlation analysis revealed a strong negative relationship between pH and nitrate removal efficiency, with a correlation coefficient of −0.97, indicating that nitrate removal decreased as pH increased. This strong inverse relationship suggests that pH significantly influenced the adsorption process. The findings are consistent with those reported by Mihayo et al. (2022), who observed maximum nitrate removal at low pH using A. digitata-derived biosorbents, and by El Ouardi et al. (2015), who reported nitrate removal efficiencies decreasing from 92.7% at pH 2 to 38% at pH 10.

Although the absolute maximum removal of 80% occurred at pH 2, maintaining strongly acidic conditions is operationally impractical and economically unfeasible for real-scale domestic wastewater treatment. Accordingly, all subsequent dosage and contact time experiments were conducted at pH 7, which is a representative of real wastewater conditions and still delivered satisfactory nitrate removal as demonstrated in subsequent sections.

4.4.2.1.2 sulphate removal

The adsorption behavior of sulphate differs fundamentally from that of nitrate due to the divalent charge of the SO_4^{2-} ion, its larger hydrated ionic radius, and its higher hydration free energy. These characteristics result in relatively larger hydration shell around sulphate compared to nitrate, making it energetically demanding for the ion to approach the adsorbent surface and undergo sufficient dehydration to form close surface contacts. At strongly acidic pH (pH 2), although the BFS-AC surface is maximally protonated and electrostatically favorable, the low pH simultaneously promotes competitive adsorption involving HSO_4^- species being the dominant form of sulphate in strong acidic conditions. In addition, the excess H^+ ions compete effectively with SO_4^{2-} for the same protonated surface sites. Furthermore, under strongly acidic conditions, surface phosphate groups

introduced during H_3PO_4 activation become protonated ($–OPO_3H_2$), reducing their ability to coordinate with SO_4^{2-} via ligand exchange.

At near-neutral pH (pH 7), the deprotonation of surface functional groups creates surface sites capable of forming stable bidentate surface complexes with SO_4^{2-} through inner-sphere coordination. This mechanism does not require a net positive surface charge and is therefore largely pH-independent in character. This observation explains why maximum sulphate removal of 40.4% occurs at pH 7, which lies above the pH at the point of zero charge (pH_pzc). Correlation analysis revealed a weak positive relationship between pH and sulphate removal efficiency, with a correlation coefficient of 0.23, indicating that pH had only a minor influence on sulphate adsorption. Despite this weak correlation, the ANOVA results ($p < 0.05$) confirmed that pH still exerted a statistically significant, although non-dominant, effect on sulphate removal.

Rahmati et al. (2019) and Salman (2009) both reported optimal sulphate adsorption under near-neutral conditions; however, neither study characterized the surface chemistry in terms of specific complexation mechanisms or functional group speciation as a function of pH. The present study addresses this gap by linking the pH-insensitive removal pattern to the inner-sphere coordination chemistry of sulphate with phosphate-modified surface groups, thereby offering a mechanistic interpretation absent from those earlier works.

4.4.2.2 Effect of adsorbent dosage on Nitrate and Sulphate removal

Adsorbent dosage was varied from 1 to 5 g per 100 mL at pH 7 with 60 minutes contact time. Results are summarised in Table 14 and shown in Figure 8.

Table 14: Effect of adsorbent dosage on nitrate and sulphate removal

Parameter	Nitrate (NO_3^-)	Sulphate (SO_4^{2-})
Dosage range tested	1–5 g / 100 mL	1–5 g / 100 mL
Optimum dosage	2 g / 100 mL	4 g / 100 mL
Max. removal at optimum	89%	75.85%
ANOVA p-value	0.00188	0.0002
Correlation coefficient (r)	-0.7	0.69
Post-optimum trend	Decline (aggregation)	Slight decline at 5 g

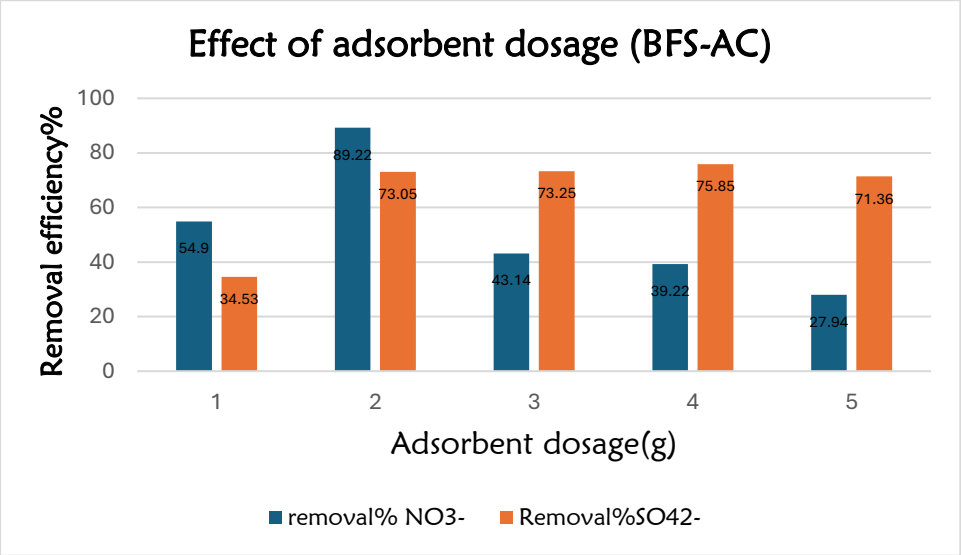


Figure 8: effect of adsorbent dosage on removal of NO_3^- and SO_4^{2-} by BFS-AC (pH=7, time=60mins, speed=150rpm)

4.4.2.2.1 Nitrate removal

Nitrate removal increased with dosage up to an optimum of 2 g per 100 mL, achieving a maximum removal efficiency of 89%. The initial increase reflects the greater availability of active adsorption sites and increased surface area at higher dosages, which enhance the probability of adsorbate–adsorbent contact. Beyond 2 g, removal declined, attributed to particle aggregation at high solid concentrations, which reduces effective surface area, and increased mass transfer resistance that limits the accessibility of nitrate ions to internal pore structures. The ANOVA result ($p = 0.00188$) confirms the dosage effect is statistically significant, while Correlation analysis showed a moderate negative relationship between dosage and nitrate removal, with a correlation coefficient (r) of -0.7, indicating that performance generally decreased as dosage increased. These findings align with El Ouardi et al. (2015), who similarly identified a post-optimum decline in nitrate removal due to overlapping of adsorption sites.

4.4.2.2.2 Sulphate removal

Sulphate removal increased sharply from 34.53% at 1 g to 73.05% at 2 g, plateaued between 2 and 3 g (73.25%), and reached a maximum of 75.85% at 4 g, before declining slightly to 71.36% at 5g. The higher optimum dosage for sulphate (4 g) compared to

nitrate (2 g) reflects the greater adsorption resistance of the divalent SO_4^{2-} ion, which requires more available surface sites to achieve comparable removal. The plateau region (2–3 g) suggests that additional dosage beyond 2 g provides diminishing returns, with the system approaching adsorption equilibrium. For subsequent contact time experiments, a uniform dosage of 2 g was selected to allow direct comparison of nitrate and sulphate kinetics under identical conditions.

4.4.2.3 Effect of contact time

All batch adsorption experiments for nitrate and sulphate removal under varying contact times were conducted at a constant pH of 7, an adsorbent dosage of 2 g, and a shaking speed of 150 rpm. The contact time was varied at 30, 60, 90, 120, and 180 minutes to evaluate its influence on adsorption performance.

The selection of 2 g adsorbent dosage for the contact time experiments was based on a balance between nitrate and sulphate removal efficiencies. Although 4 g was identified as the optimum dosage for sulphate removal, 2 g was selected because it provided satisfactory removal efficiencies for both nitrate and sulphate simultaneously, whereas 4 g favoured sulphate removal only. Therefore, 2 g was considered more appropriate for comparative evaluation of adsorption kinetics for both ions under the same operating conditions. Results are presented in Table 15 and Figure 9.

Table 15: Effect of contact time on nitrate and sulphate removal at pH 7, 2 g dosage

Contact Time (min)	Nitrate Removal (%)	Sulphate Removal (%)	Stage
30	38.69	45.53	Rapid initial uptake
60	88.94	82.42	Approaching equilibrium
90	90.45	88.14	Equilibrium reached
120	80.40	81.10	Onset of desorption
180	60.30	78.19	Continued desorption

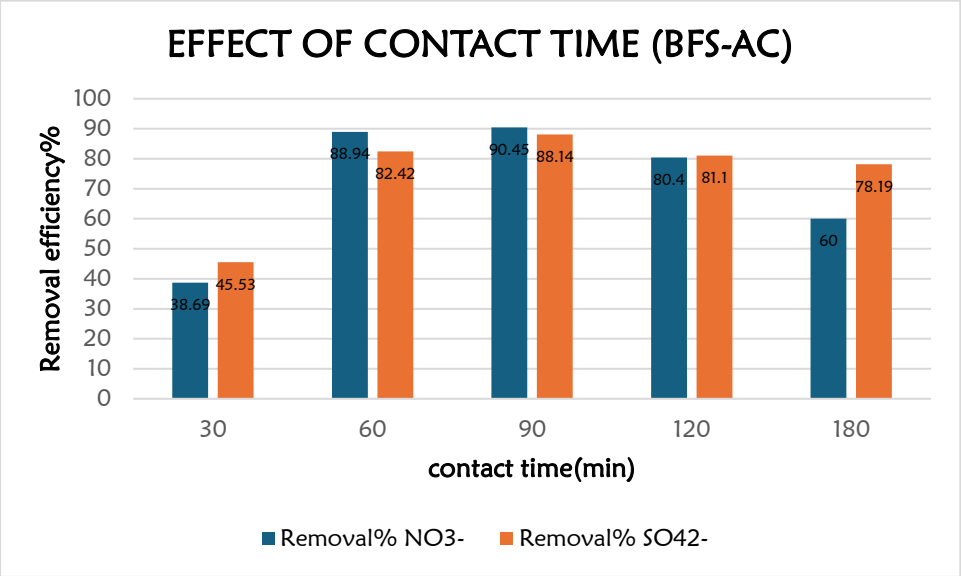


Figure 9: effect of contact time on removal of NO3- and SO42- by BFS-AC (pH=7, dosage=2g, speed=150rpm)

4.4.2.3.1 Nitrate

Nitrate removal increased rapidly from 38.69% after 30 minutes to 88.94% after 60 minutes, reaching a maximum of 90.45% at 90 minutes. Beyond this point, removal efficiency declined to 80.4% at 120 minutes and further to 60.3% at 180 minutes. The sharp initial rise can be attributed to the substantial concentration gradient between the nitrate ions in solution and the adsorbent surface, coupled with the abundance of vacant adsorption sites during the early stage of the experiment. As contact time progresses and these sites become increasingly occupied, the adsorption rate gradually decreases, and the system moves toward equilibrium.

Equilibrium is defined as the state at which the adsorption rate equals the desorption rate, resulting in no net change in the adsorbate concentration in solution. In the present study, equilibrium for nitrate was achieved at 90 minutes, as indicated by the maximum removal efficiency and the subsequent post-equilibrium decline. The drop in removal efficiency beyond 90 minutes is thought to result from desorption: weakly physiosorbed nitrate ions, retained through reversible electrostatic interactions, are released back into solution as continued agitation and competition for surface sites disturb the equilibrium. This desorption behavior supports the role of physisorption as a contributing mechanism in nitrate removal by BFS-AC.

4.4.2.3.2 Sulphate

Sulphate removal followed a similar temporal pattern, increasing from 45.53% at 30 minutes to 82.42% at 60 minutes and reaching a maximum of 88.14% at 90 minutes. Post-equilibrium values were 81.10% (120 min) and 78.19% (180 min). The convergence of equilibrium times for both nitrate and sulphate at 90 minutes suggests that pore diffusion is a common rate-limiting step for both ions, regardless of their different adsorption mechanisms.

The more gradual post-equilibrium declines for sulphate compared to nitrate (88.14% to 78.19% vs. 90.45% to 60.3% over the same interval) suggests that sulphate is more strongly bound to the BFS-AC surface consistent with the chemical complexation mechanism proposed in Section 4.4.2.1.2, where SO_4^{2-} forms more stable surface complexes that resist desorption more effectively than the electrostatically adsorbed NO_3^-. The equilibrium time of 90 minutes is operationally practical and consistent with contact times reported in comparable activated carbon studies (60–120 minutes).

4.5 ADSORPTION KINETICS

Adsorption kinetics describe the rate at which adsorbate ions are removed from solution and the mechanism controlling that rate (Vunain et. al, 2019). Understanding kinetics is essential for predicting how quickly equilibrium is reached and for designing treatment systems with appropriate contact times. In this study, the pseudo-first-order (PFO) and pseudo-second-order (PSO) kinetic models were applied to the contact time data obtained at pH 7 with an adsorbent dosage of 2 g per 100 ml. The adsorption capacity at each time point (q_t, mg/g) was calculated using Equation 4.2:

$$q_t = (C_0 - C_t) \times V / m \quad \ldots \text{(Equation 4.2)}$$

Where C_0 is the initial concentration (mg/L), C_t is the concentration at time t (mg/L), V is the volume of solution (L), and m is the mass of adsorbent (g). Using C_0 = 36 mg/L for nitrate (synthetic sample) and C_0 = 46.4955 mg/L for sulphate (based on measured initial effluent concentration), the q_t values at each time point are presented in Table 16.

Table 16: Calculated q_t values at each contact time for nitrate and sulphate (pH 7, 2 g/100 mL)

Time (min)	NO_3^- RE (%)	NO_3^- C_t (mg/L)	NO_3^- q_t (mg/g)	SO_4^{2-} RE (%)	SO_4^{2-} C_t (mg/L)	SO_4^{2-} q_t (mg/g)
30	38.69	21.97	0.7012	45.53	25.326	1.058470
60	88.94	3.98	0.6403	82.42	8.174	1.916080
90	90.45	3.44	0.6512	88.14	5.514	2.049057
120	80.40	7.06	0.5747	81.10	8.788	1.885393
180	60.30	14.29	0.4310	78.19	10.141	1.817742

4.5.1 Pseudo-First-Order Model

The pseudo-first-order (PFO) model originally proposed by Lagergren in 1898, assumes that the rate of adsorption is proportional to the number of unoccupied adsorption sites and is generally associated with physical adsorption (Chu, Bolinger, & Kierczak, 2025). The linearised form of the PFO model is given by Equation 4.3:

$$\ln (q_e - q_t) = \ln(q_e) - k_1 t \quad \ldots \text{(Equation 4.3)}$$

where q_e is the equilibrium adsorption capacity (mg/g), q_t is the adsorption capacity at time t (mg/g), and k_1 is the pseudo-first-order rate constant (min^{-1}). A plot of $\ln (q_e - q_t)$ versus t yields a straight line with slope $-k_1$ and intercept $\ln(q_e)$. This linearisation is valid only for pre-equilibrium time points (t = 30, 60, and 90 min), as at and beyond equilibrium $q_t \geq q_e$, rendering $\ln (q_e - q_t)$ undefined.

The PFO model yielded rate constants of k_1 = -0.0032min^{-1} for nitrate and k_1 = 0.0064min^{-1} for sulphate. The calculated equilibrium adsorption capacities were q_e =0.223 mg/g (nitrate) and q_e = 0.497 mg/g (sulphate), with coefficients of determination R^2 =0.0143 nitrate and R^2 = 0.222 for sulphate. However, the calculated q_e values deviate appreciably from the experimentally determined equilibrium capacities of q_e = 0.651 mg/g (nitrate) and q_e = 2.049 mg/g (sulphate), confirming that the PFO model does not adequately describe the adsorption of either ion onto BFS-AC. The linearisation data for the PFO model are presented in Table 17.

Table 17: Pseudo-first-order linearisation data, ln ($q_e - q_t$) versus t

Time (min)	q_t NO_3^-	$q_e - q_t$ NO_3^-	$\ln(q_e - q_t)$ NO_3^-	q_t SO_4^{2-}	$q_e - q_t$ SO_4^{2-}	$\ln(q_e - q_t)$ SO_4^{2-}
30	0.7012	-0.0500	—	1.058470	0.990587	−0.0095
60	0.6403	0.0109	−4.5181	1.916080	0.132977	−2.0176
90	0.6512	0.0000	—	2.049057	0.0000	—
120	—	—	—	—	—	—
180	—	—	—	—	—	—

Note: Values at t = 90 min yield $q_e - q_t = 0$ and are therefore excluded from linearisation. Values at t = 120 and 180 min are excluded as q_t exceeds q_e post-equilibrium.

4.5.2 Pseudo-Second-Order Model

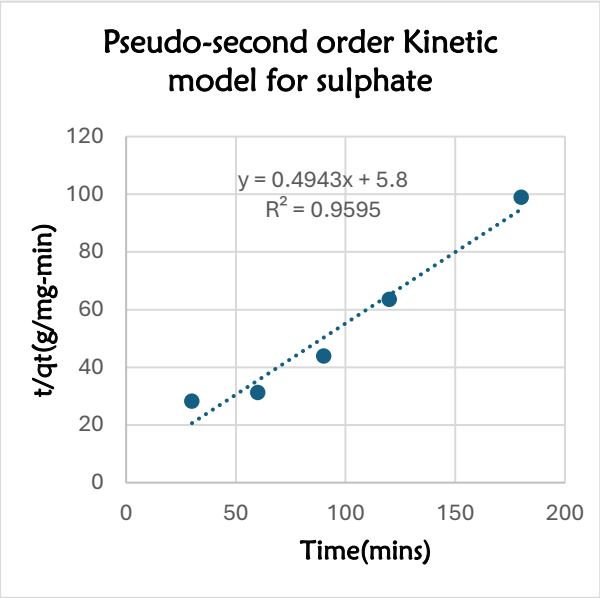
The pseudo-second-order (PSO) model (Ho & McKay, 1999) assumes that the rate-limiting step in the adsorption process involves chemisorption the formation of chemical bonds between adsorbate ions and reactive functional groups on the adsorbent surface. The linearised form of the PSO model is given by Equation 4.4:

$$t/q_t = 1/(k_2 q_e^2) + t/q_e \quad \ldots \text{(Equation 4.4)}$$

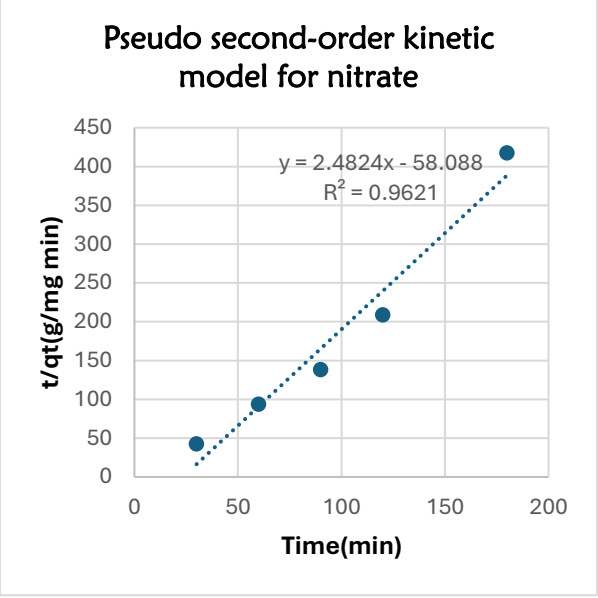
where k_2 is the pseudo-second-order rate constant (g/mg·min). A plot of t/q_t versus t yields a straight line with slope $1/q_e$ and intercept $1/(k_2 q_e^2)$, from which both q_e and k_2 can be determined. Unlike the PFO model, the PSO linearisation can be applied to all five time points as t/q_t is always defined. The data are presented in Table 18 and Figure 10.

Table 18: Pseudo-second-order linearisation data t/q_t versus t

t (min)	NO_3^- q_t (mg/g)	t/q_t NO_3^- (min·g/mg)	SO_4^{2-} q_t (mg/g)	t/q_t SO_4^{2-} (min·g/mg)
30	0.7012	42.78	1.058470	28.34
60	0.6403	93.70	1.916080	31.31
90	0.6512	138.21	2.049057	43.92
120	0.5747	208.80	1.885393	63.65
180	0.4310	417.63	1.817742	99.02



(a)



(b)

Figure 10: showing plot for PSO for (a) sulphate and (b) nitrate

The PSO model yielded a rate constant of k_2 = 0.04 g/mg·min for sulphate and k_2=-0.00312/mg.min, with a calculated equilibrium capacity q_e = 2.023 mg/g for sulphate and q_e = 0.648mg/g for nitrate closely matching the experimental value of 2.049 mg/g for sulphate and 0.651 mg/l for nitrate. The PSO model achieved R^2=0.9595 for sulphate and R^2=0.9621 for nitrate. A comparison of both models is presented in Table 19.

Table 19: Comparison of pseudo-first-order and pseudo-second-order kinetic model parameters

Parameter	PFO NO_3^-	PFO SO_4^{2-}	PSO NO_3^-	PSO SO_4^{2-}
Rate constant	k_1 = 0.0032 min^{-1}	k_1 = 0.0064 min^{-1}	k_2 = 0.00312 /mg.min	k_2 = 0.040 g/mg·min
Calc. q_e (mg/g)	0.223	0.497	0.648	2.023
Exp. q_e (mg/g)	0.651	2.049	0.651	2.049
R^2	0.0146	0.222	0.9621	0.9595
Best fit?	No	No	Yes	Yes

The superior fit of the PSO model ($R^2 > 0.95$ for both ions) and the close agreement between calculated and experimental q_e values confirm that chemisorption is the dominant rate-controlling mechanism for both nitrate and sulphate adsorption onto BFS-AC. This is consistent with the presence surface functional groups, and phosphate groups introduced by H_3PO_4 activation, which facilitate chemical complexation with anions in solution.

4.6 ADSORPTION ISOTHERMS

Adsorption isotherm models describe the equilibrium relationship between the concentration of adsorbate remaining in solution at equilibrium (Ce) and the amount adsorbed per unit mass of adsorbent (qe) at constant temperature (Ali, Sadek, & Mansi, 2021). Isotherm studies are important because they provide insight into the adsorption capacity, surface characteristics of the adsorbent, and the interaction between adsorbate ions and active adsorption sites. The Langmuir and Freundlich isotherm models were applied to characterise the adsorption equilibrium of nitrate and sulphate onto BFS-AC.

Isotherm experiments were conducted using synthetic samples at pH 7, adsorbent dosage of 2 g, and contact time of 90 minutes, with initial concentrations varying from 25–45 mg/L for sulphate and 30–70 mg/L for nitrate. The equilibrium data are presented in Table 20.

Table 20: Equilibrium adsorption data from multi-concentration isotherm experiments (pH 7, 2 g, 90 min)

SO_4^{2-} C_0 (mg/L)	SO_4^{2-} Ce (mg/L)	SO_4^{2-} q_e (mg/g)	NO_3^- C_0 (mg/L)	NO_3^- C_e (mg/L)	NO_3^- q_e (mg/g)
25	3.12	1.09	30	2.66	1.37
30	5.08	1.25	40	5.00	1.75
35	8.99	1.30	50	7.80	2.11
40	11.00	1.45	60	12.10	2.40
45	12.67	1.62	70	14.89	2.76

4.6.1 Langmuir Isotherm

The Langmuir isotherm is the model most commonly used in equilibrium studies of biosorption. However, while it remains popular for such applications, it provides little information regarding the underlying mechanisms of the adsorption process (Alafnan et.al, 2021). The model is based on the assumption that adsorption takes place as a single layer on a uniform adsorbent surface composed of identical sites. Additionally, it presumes that all of these sites have the same adsorption energy and that there are no interactions between the molecules once they are adsorbed (Langmuir, 1916). The linearised form is given by Equation 4.5:

$$C_e/q_e = 1/ (Q_{max} \cdot KL) + C_e/Q_{max} \quad \text{... (Equation 4.5)}$$

Where q_e is the monolayer adsorption capacity of adsorbent(mg/g), Ce is the equilibrium concentration(mg/l), Q_{max} is the theoretical maximum monolayer adsorption capacity (mg/g) and KL is the Langmuir equilibrium constant related to the energy of adsorption (L/mg). A plot of C_e/q_e versus C_e gives a straight line with slope $1/Q_{max}$ and intercept $1/ (Q_{max} \cdot KL)$.

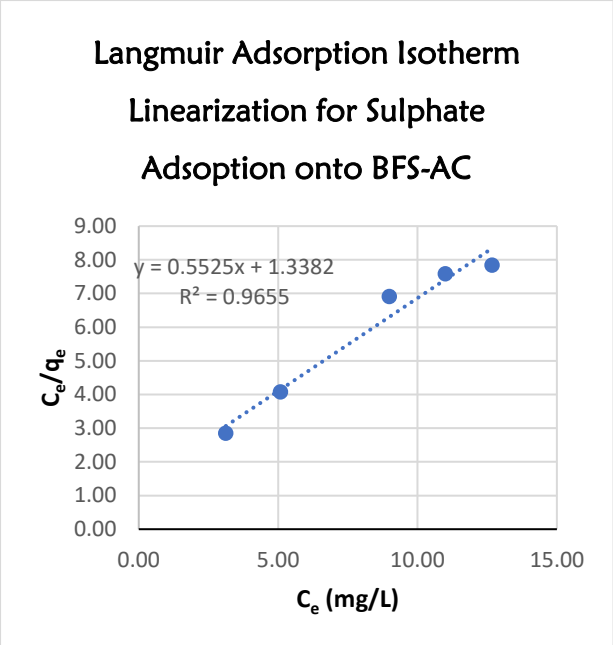
The suitability of the Langmuir model is further evaluated using the dimensionless separation factor RL (Equation 4.6), which indicates whether adsorption is favourable ($0 < RL < 1$), unfavourable ($RL > 1$), linear ($RL = 1$), or irreversible ($RL = 0$):

$$RL = 1 / (1 + KL \cdot C_0) \quad \text{.... (Equation 4.6)}$$

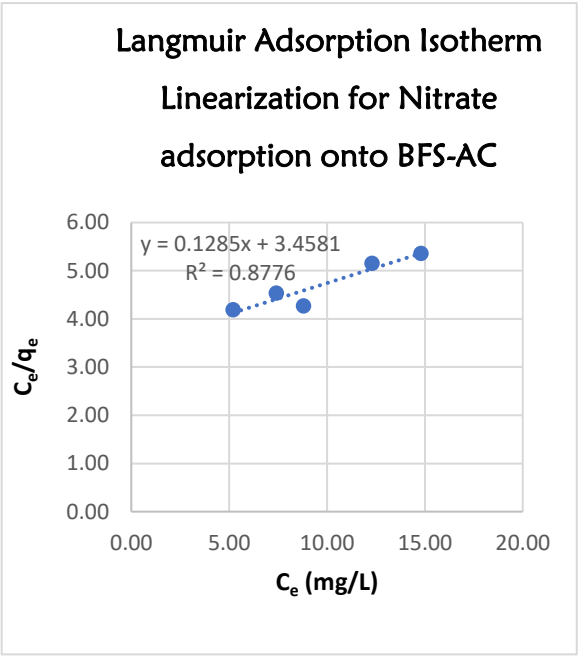
The Langmuir model yielded a maximum adsorption capacity Q_{max} = 7.782 mg/g and KL = 0.037 L/mg for nitrate, and Q_{max} = 3.476 mg/g and KL = 0.213 L/mg for sulphate, with R^2 = 0.966 (sulphate) and R^2 = 0.878 (nitrate). The separation factors were ranging from (0.374 – 0.518) for nitrate and a range of (0.063 – 0.135) for sulphate, both falling within the range $0 < RL < 1$, confirming that the Langmuir model predicts favourable adsorption for both ions under the initial concentrations studied but with excellent fit for sulphate as compared to nitrate with respect to the R^2 values. The Langmuir linearisation parameters are summarised in Table 21.

Table 21: Langmuir isotherm parameters for nitrate and sulphate adsorption onto BFS-AC

Parameter	Nitrate (NO^{-}_{3})	Sulphate (PO^{2-}_{4})
q_{max}	7.782	3.476
K_L	0.037	0.213
RL	(0.374 - 0.518)	(0.063 - 0.135)
R^2	0.878	0.966
Adsorption type	Favourable (0 < RL < 1)	Favourable (0 < RL < 1)



(a)



(b)

Figure 11: Langmuir adsorption isotherms for (a) sulphate and (b) nitrate

4.6.2 Freundlich Isotherm

According to Ehiomogue et.al, (2022), the Freundlich isotherm describes sorption on a heterogeneous surface where interactions occur between adsorbed molecules. Applying the Freundlich equation implies that the adsorption energy declines exponentially as the

adsorbent's active sites become occupied. This isotherm points to the presence of adsorption-complexation reactions during the sorption process. The linearised form is given by Equation 4.7:

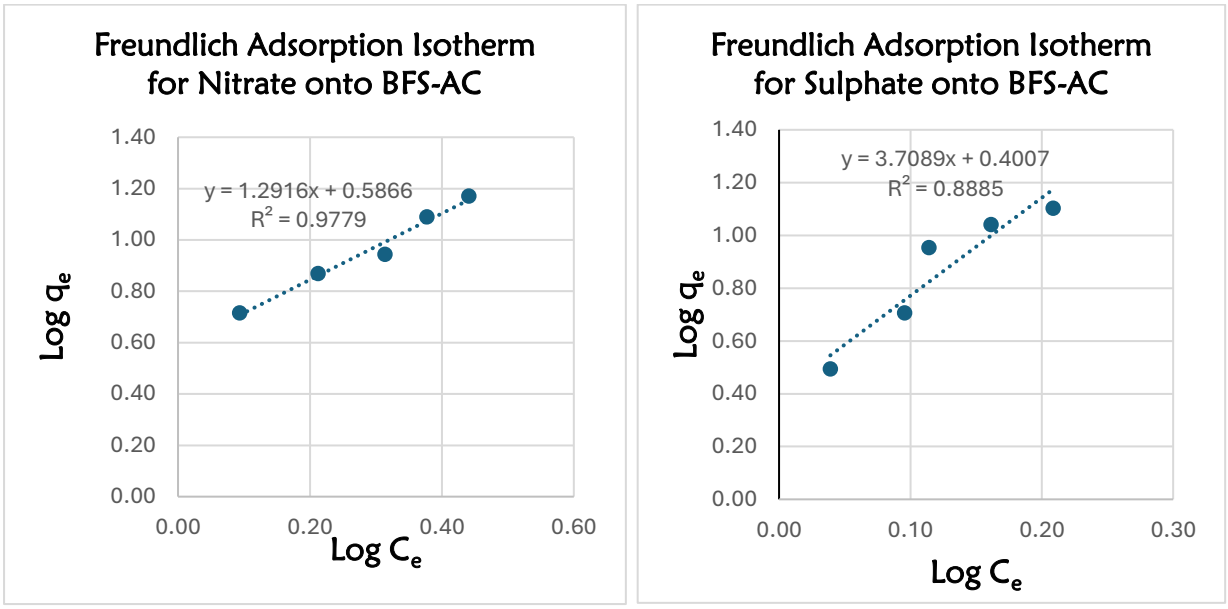
$$\log(q_e) = \log(Kf) + (1/n) \cdot \log(C_e) \quad \ldots(\text{Equation 4.7})$$

Where q_e is the equilibrium adsorbate uptake per unit mass of adsorbent (mg/g), and C_e is the equilibrium adsorbate concentration in solution (mg/L), Kf (mg/g) $(L/mg)^{(1/n)}$ and n are Freundlich constants which represent adsorption capacity and adsorption intensity and 1/n is referred to as the adsorption intensity parameter. A linear plot of log qe against log*Ce* gives a slope of 1/n and an intercept of log*Kf*. In this study, Kf and n were derived from the intercept and slope of the log*qe* versus log *Ce* plot, respectively.

The Freundlich model yielded Kf = 3.86 (mg/g) (L/mg) ^ (1/n) and 1/n = 1.292 for nitrate, and Kf = 2.520 and 1/n = 3.7089 for sulphate, with R^2 = 0.9779 (nitrate) and R^2 = 0.8885 (sulphate). The Freundlich parameters are summarised in Table 22.

Table 22: Freundlich isotherm parameters for nitrate and sulphate adsorption onto BFS-AC.

Parameter	Nitrate	Sulphate
Kf $(mg/g)(L/mg)^{1/n}$	3.86	2.52
1/n	1.292	3.7089
R^2	0.9779	0.8885
Surface type indicated	heterogenous favourable	heterogenous favourable



(a) (b)

Figure 12: Freundlich adsorption isotherms for (a) Nitrate and (b) Sulphate

The relatively high correlation coefficients obtained for nitrate ($R^2 = 0.9779$) and sulphate ($R^2 = 0.8885$) indicate that the Freundlich model adequately described the adsorption process, particularly for nitrate. This suggests that adsorption occurred on a heterogeneous adsorbent surface with adsorption sites having different energy levels.

The Freundlich constant, Kf, which represents adsorption capacity, was higher for nitrate (3.86 mg/g (L/mg)$^{1/n}$) than for sulphate (2.52 mg/g (L/mg)$^{1/n}$). This indicates that BFS-AC had a greater adsorption affinity and capacity for nitrate ions compared to sulphate ions. The higher Kf value for nitrate implies stronger interaction between nitrate ions and the active sites on the adsorbent surface.

4.6.3 Comparison of Isotherm Models

Both the Langmuir and Freundlich models provided acceptable fits to the equilibrium data, with the Langmuir model yielding slightly higher R^2 values for sulphate (0.965), indicating that adsorption mainly occurred through monolayer adsorption on relatively homogeneous active sites of the BFS-AC surface. This supports the sulphate removal process as dominated by chemosorption. Since nitrate is a monovalent ion with lower charge density, its adsorption is generally weaker and more associated with physical adsorption and indicated by its best fit with Freundlich adsorption isotherm.

The Langmuir behavior also complements the pseudo-second-order kinetic model obtained previously. Since pseudo-second-order kinetics are commonly associated with chemisorption involving electron sharing or electron exchange mechanisms, the combined Langmuir and kinetic results provide strong evidence that sulphate adsorption was predominantly chemically driven rather than purely controlled by electrostatic attraction. These findings are consistent with ranges reported for H_3PO_4-activated agricultural-waste carbons in the literature (Salman, 2009; Rahmati et al., 2019), further validating the practical adsorption potential of BFS-AC under the conditions of this study.

4.7 Comparative Performance with Published Studies

The adsorption performance of BFS-AC in removing nitrate and sulphate from domestic wastewater is compared with published values from BFS-based and other agricultural-waste-derived activated carbons in Table 23.

Table 23: Comparative adsorption performance for nitrate and sulphate removal

Study	Adsorbent	Ion	Max. Removal (%)	Opt. pH
This study	BFS-AC (H_3PO_4)	NO_3^-	90.45	7 (practical)
This study	BFS-AC (H_3PO_4)	SO_4^{2-}	88.14	7
Mihayo et al. (2022)	A. digitata pericarp	NO_3^-	88.95	2
El Ouardi et al. (2015)	New clay	NO_3^-	71.89	5.1
Adebayo et al. (2016)	Activated carbon	NO_3^-	Comparable	Low pH
Rahmati et al. (2019)	Ziziphus spina-Christi lotus leaf	SO_4^{2-}	84.5	6
Salman (2009)	Activated carbon	SO_4^{2-}	43.0	7

The nitrate removal of 90.45% achieved in this study at pH 7 is competitive with the literature and surpasses several studies that report maximum removal only under strongly acidic conditions impractical for real-world conventional wastewater treatment. The sulphate removal of 88.14% is notably higher than Salman (2009) (43%) and exceeds Rahmati et al. (2019) (84.5%), representing one of the stronger sulphate removal efficiencies reported for an unmodified, low-cost agricultural-waste-derived carbon. Critically, these results were achieved using real domestic wastewater rather than the synthetic single-ion solutions used in most comparable studies. In real wastewater, competitive adsorption among multiple ions simultaneously present in solution is expected to reduce individual removal efficiencies; the high efficiencies observed despite this competitive environment therefore underscore the adsorption capacity and practical effectiveness of the prepared BFS-AC. Compared to BFS-AC studies focused on other pollutants, Vunain et al. (2017) achieved 93.1% Cu (II) removal and Vunain & Biswick (2019) reported 99.5% methylene blue removal. The present study extends the known application scope of BFS-AC to inorganic anion removal, which represents a critical but previously underexplored use case for this material under Malawian conditions.

CHAPTER 5: CONCLUSION AND RECOMMENDATIONS

5.1 CONCLUSION

The study evaluated the efficiency of raw baobab fruit shell adsorbent and baobab fruit shell-derived activated carbon (BFS-AC) in the removal of inorganic anions from domestic wastewater. The characterization results showed that BFS-AC possessed improved adsorption properties compared to the raw adsorbent, including higher iodine number, increased porosity, and lower moisture and ash content, indicating successful activation and enhanced adsorption potential.

Batch adsorption experiments demonstrated that both the raw baobab shell adsorbent and BFS-AC were capable of removing nitrate and sulphate ions from wastewater, although BFS-AC achieved higher removal efficiencies due to its improved surface properties and pore development. Nitrate adsorption was strongly influenced by pH and was favored under acidic conditions due to electrostatic attraction, while sulphate adsorption was less dependent on pH and was favored near neutral conditions, suggesting stronger surface interactions.

Adsorption modelling showed that pseudo-second-order kinetics best described both nitrate and sulphate adsorption, indicating the importance of surface interactions in the adsorption process. Freundlich isotherm best fitted nitrate adsorption, suggesting heterogeneous adsorption, while Langmuir isotherm best fitted sulphate adsorption, indicating monolayer adsorption on relatively uniform active sites.

Overall, the findings demonstrate that baobab fruit shells, particularly in activated form, are low-cost, sustainable, and effective adsorbents for the removal of inorganic anions from domestic wastewater, with potential application in wastewater treatment systems in Malawi.

5.2 RECOMMENDATIONS

Further studies should be conducted at pilot scale and under continuous flow conditions to evaluate the practical application of baobab fruit shell-derived activated carbon (BFS-AC) in real wastewater treatment systems. Future research should also investigate the regeneration and reusability of BFS-AC in order to assess its long-term operational and economic feasibility. In addition, further research should also explore the efficiency of BFS-AC in removing other inorganic and organic pollutants from wastewater. Lastly, wastewater treatment facilities and environmental stakeholders should consider the use of low-cost agricultural waste-based adsorbents as sustainable alternatives to commercial activated carbon for improving wastewater treatment efficiency in Malawi.

REFERENCES

Adonadaga, M. (2019). *Domestic Wastewater Characterization and Potential for Treatment Using Close-to-Nature Methods*. *9*(3), 51–59. https://doi.org/10.7176/JEES

Alafnan, S., Awatunde, A. A., Glatz, G., & Stephen, A. (2021, june). Langmuir adsoption in unconventional resources: Applicability and limitation.

Ali, D. A., Sadek, M. A., & Mansi, N. M. (2021, october). Isotherm and kinetics study for the adsorption of nitrate and phospahet ions from aquous solutions using fume dust from electric ARC furnace. *16*.

Ali, I., Asim, M., & Khan, A. T. (2012, December 30). Low cost adsorbents for the removal of organic pollutants from wastewater. *113*, 170-183. Retrieved from https://doi.org/10.1016/j.jenvman.2012.08.028

avi, P., & Kumari, S. (2024). Eutrophication: Understanding and Mitigating Eutrophication in Pond Water. *International Journal of Current Microbiology and Applied Sciences*, *13*(11), 21–25. https://doi.org/10.20546/IJCMAS.2024.1311.003

Ayach, J., El Malti, W., Duma, L., Lalevée, J., Al Ajami, M., Hamad, H., & Hijazi, A. (2024). Comparing Conventional and Advanced Approaches for Heavy Metal Removal in Wastewater Treatment: An In-Depth Review Emphasizing Filter-Based Strategies. *Polymers*, *16*(14), 1959. https://doi.org/10.3390/POLYM16141959

Ayers, R. S., & Westcot, D. W. (2024). *Water quality for agriculture - 6. WATER QUALITY FOR LIVESTOCK AND POULTRY*. 1–5. https://www.fao.org/4/T0234E/T0234E00.htm#TOC

Bhatnagar, A., Hogland, W., Marques, M., & Sillanpaa, M. (2013, March). an overview of the modified methods of activated carbon for its water treatment applications. doi:10.1016/j.cej.2012.12.038

Chidulo, G. W. (2019). wastewater disposal status in Malawi Based on the city of Blantyre as Acase study (Doctoral dissertation, University of Malawi- The Polytechnic).

Chu, K., Bolinger, J.-c., & Kierczak. (2025, December). pseudo-first order kinetics in environmental adsorption; why are there two distict equation? *3*, 191-195. Retrieved from https://doi.org/10.1016/j.esi.2025.07.001

Daffalla, S. (2025). Removal of Malachite Green Dye from Aqueous Solution by a Novel Activated Carbon Prepared from Baobab Seeds Using Chemical Activation Method. *Molecules*, *30*(2). https://doi.org/10.3390/MOLECULES30020407

Debbache, H., Ayachi Amor, A., Zohra, F., Amor, A., Khiari, R., Moussaoui, Y., Lakhdar Belfar, M., Moussaoui, Y., & Zerrouki, H. (2024). a comprehensive analysis of the use of chemical activation technology to produce activated carbon from agricultural residues. *cellulose chemistry and technology Cellulose Chem. Technol*, *58*(9), 1149–1161.

Ehiomogue, P., Ahuchaogu, I., & Ahaneku, I. (2022, February). Review of adsorption isotherm models.

Fröhlich, A. C., Ocampo-Pérez, R., Diaz-Blancas, V., Salau, N. P. G., & Dotto, G. L. (2018). Three-dimensional mass transfer modelling of ibuprofen adsorption on activated carbon prepared by sonication. *Chemical Engineering Journal*, *341*, 65–74. https://doi.org/10.1016/J.CEJ.2018.02.020

Izabella, M., kamil, N., Piotr, P., & Jorg, M. (2025, May). Biomass Ash: Areview of chemical composition and management trend. doi:10.3390/su17114295

Hossain, Md. Z., Chowdhury, M. B. I., Hossain, Md. Z., & Chowdhury, M. B. I. (2024). Biobased Activated Carbon and Its Application. *Biomass Based Products*. https://doi.org/10.5772/INTECHOPEN.1008374

Jere, E. (2024). *evaluating the performance of livingstonia wastewater stabilization ponds and their effects on mpopi stream in rumphi, malawi*.

Jodar-Abellan, A., López-Ortiz, M. I., & Melgarejo-Moreno, J. (2019). Wastewater Treatment and Water Reuse in Spain. Current Situation and Perspectives. *Water 2019, Vol. 11, Page 1551*, *11*(8), 1551. https://doi.org/10.3390/W11081551

Kayira, F., & Wanda, E. M. M. (2021). Evaluation of the performance of Mzuzu Central Hospital wastewater oxidation ponds and its effect on water quality in Lunyangwa

River, Northern Malawi. *Physics and Chemistry of the Earth*, *123*. https://doi.org/10.1016/j.pce.2021.103015

Kamalesh, S., Shovan, M., & Mondal, N. K. (2026, April). surface charge behaviour of natural and modified adsorbents: insights into PHpzc, mechanisms and methedological perspectives. *11*. Retrieved from https://doi.org/10.1016/j.nxmate.2026.10198

Khamkeaw, A., Tatdanai, A., Perngyai, T., & Jongsongmjit, B. (2020, september). interconnected micro,meso and macro porous activated carbon from bacterial nanocellulose for superior Adsorption properties and effective catalytic perfomance.

Kodzwa, J., Danha, C., Mangori, L., & Chemura, A. (2015). Activated carbon from baobab fruit shells through domestic processes. *Zimbabwe Journal of Technological Sciences*, *1*(January 2015), 19–28. https://www.researchgate.net/publication/286019316%0Ahttps://www.researchgate.net/publication/286019316_Activated_carbon_from_baobab_fruit_shells_through_domestic_processes

Lakshmi, K. S., & Reddy, M. A. (2017). Wastewater - An overview. *International Journal of Contemporary Research and Review*. https://doi.org/10.15520/IJCRR/2017/8/08/287

Lu, Z., Sun, W., Li, C., Cao, W., Jing, Z., Li, S., Ao, X., Chen, C., & Liu, S. (2020). Effect of granular activated carbon pore-size distribution on biological activated carbon filter performance. *Water Research*, *177*, 115768. https://doi.org/10.1016/J.WATRES.2020.115768

Lundgren, S. (2013). *Efficiency of two wastewater treatment plants situated in Zomba, Malawi*. https://www.diva-portal.org/smash/get/diva2:629901/FULLTEXT01.pdf

Malikula, R. S., Kaonga, C. C., Mapoma, H. W. T., Chiipa, P., & Thulu, F. G. D. (2022). Heavy Metals and Nutrients Loads in Water, Soil, and Crops Irrigated with Effluent from WWTPs in Blantyre City, Malawi. *Water (Switzerland)*, *14*(1). https://doi.org/10.3390/W14010121

Mdolo, P. (2017). *treatment efficacy of kauma wastewater treatment works in lilongwe , malawi for pollution control and wastewater reuse principal mdolo (NRC). October*.

Mihayo, D., Vegi, M. R., & Vuai, S. A. H. (2022). Attenuation of nitrate from aqueous solution using raw and surface modified biosorbents from Adansonia digitata fruit pericarp. *Heliyon*, *8*(8). https://doi.org/10.1016/J.HELIYON.2022.E10004

Ndiaye, E. M., Ba, K., Sow, A., Diop, A., Idrissi, Y. El, Moudden, H. El, Faye, P. G., Harhar, H., Ayessou, N., Tabyaoui, M., & Cisse, M. (2022b). Valorization of Natural Residue into Activated Carbon: Example of the Shells of the African Baobab Fruit (Adansonia digitata) L. *Journal of Materials Science and Engineering A*, *12*(6), 41–54. https://doi.org/10.17265/2161-6213/2022.4-6.001

Nedjai, R., Alkhatib, M. F. R., Alam, M. Z., & Kabbashi, N. A. (2021). Adsorption Of Methylene Blue Onto Activated Carbon Developed From Baobab Fruit Shell By Chemical Activation: Kinetic Equilibrium Studies. *IIUM Engineering Journal*, *22*(2), 31–49. https://doi.org/10.31436/IIUMEJ.V22I2.1682

Nedjai, R., Kabbashi, N. A., Alam, M. Z., & Al-Khatib, M. F. R. (2021). Production and Characterization of Activated Carbon from Baobab Fruit Shells by Chemical Activation Using ZnCl2, H3PO4 and KOH. *Journal of Physics: Conference Series*, *2129*(1). https://doi.org/10.1088/1742-6596/2129/1/012009

Nedjai, R., Kabbashi, N. A., Alam, M. Z., & Alkhatib, M. F. R. (2022). optimisation of activated carbon production from baobab fruit shells by chemical activation with koh for the removal of phenol. *Water Conservation and Management*, *6*(1), 45–50. https://doi.org/10.26480/WCM.01.2022.45.50

Nedjai, R., Kabbashi, N. A., Alkhatib, M. F. R., & Alam, M. Z. (2021). Removal of Phenol from Aqueous Solution by Adsorption onto Baobab Fruit Shell Activated Carbon : Equilibrium and Kinetics Studies. *Journal of Environmental Treatment Techniques*, *9*(3), 686–697. https://doi.org/10.47277/JETT/9(3)697

Njewa, J. B., & Shikuku, V. O. (2023). Recent advances and issues in the application of activated carbon for water treatment in Africa: A systematic review (2007–2022). *Applied Surface Science Advances*, *18*, 100501. https://doi.org/10.1016/J.APSADV.2023.100501

Oloriegbe, T., Okofu, C. A., & Ibrahim, F. B. (2022). The Use of Selected Carbonized Agricultural Waste as a Low Cost Scrubber in Air Pollution Control. *Romanian Journal of Transport Infrastructure*, *11*(2), 1–17. https://doi.org/10.2478/RJTI-2022-0012

Pet, I., Sanad, M. N., Farouz, M., ElFaham, M. M., El-Hussein, A., El-sadek, M. S. A., Althobiti, R. A., & Ioanid, A. (2024). Review: Recent Developments in the Implementation of Activated Carbon as Heavy Metal Removal Management. *Water Conservation Science and Engineering*, *9*(2), 1–15. https://doi.org/10.1007/S41101-024-00287-3/FIGURES/3

Pereira, R. C., Arbestain, M. C., Kaal, J., & Lorenzo, R. P. (2011, october). Contribution to characterisation of biochar to estimate labile fraction of carbon. doi:10.1016/j.orggeochem.2011.09.002

Phothong, K., Tangsanthitkulcga, C., & Lawtae, P. (2021, august 23). Analysis of pore development and formation of surface functional groups in bamboo based activated carbon during CO2 activation.

Rajasulochana, P., & Preethy, V. (2016, December). Comparison on efficiency of various techniques in treatment of waste and sewage water- A comprehensive review. *2*(4), 175-184. Retrieved from https://www.sciencedirect.com/science/article/pii/S2405653716301683#:~:text=Some%20techniques%20deal%20with%20reduction,Background%20information

Reza, M. S., Yun, C. S., Afroze, S., Radenahmad, N., Bakar, M. S. A., Saidur, R., Taweekun, J., & Azad, A. K. (2020). Preparation of activated carbon from biomass and its' applications in water and gas purification, a review. *Arab Journal of Basic and Applied Sciences*,*27*(1), 208–238. https://doi.org/10.1080/25765299.2020.1766799;JOURNAL:JOURNAL:TABS19;PAGE:STRING:ARTICLE/CHAPTER

Shang, Z., Yang, Z., & Ma, Y. (2023a). Theoretical study of activated carbon production via a two-step carbonization-activation process based on Aspen Plus calculation. *Biomass Conversion and Biorefinery*, *13*(9), 8267–8276. https://doi.org/10.1007/S13399-021-01687-4

Sadeghalvad, B., Khorshidi, N., Sillanpaa, M., & Azadmehr, A. (2021, january). Sorption, mechanism and behaviour of sulphates on various adsorbents: a critical review. *263*.

Sharma, G., Sharma, S., Stadler, F. J., Kumar, A., Lai, C. W., & Iqbal, J. (2022, january 01). Activated carbon as superadsorbent and sustainable material for diverse applications. doi:https://doi.prg/10.1155/2022/4184809

Shi, Q., Zhang, S., Xie, M., Christodoulatos, C., & Meng, X. (2022). Competitive adsorption of nitrate, phosphate, and sulfate on amine-modified wheat straw: In-situ infrared spectroscopic and density functional theory study. *Environmental Research*, *215*, 114368. https://doi.org/10.1016/J.ENVRES.2022.114368

Soffian, M. S., Abdul Halim, F. Z., Aziz, F., A. Rahman, M., Mohamed Amin, M. A., & Awang Chee, D. N. (2022). Carbon-based material derived from biomass waste for wastewater treatment. *Environmental Advances*, *9*, 100259. https://doi.org/10.1016/J.ENVADV.2022.100259

Soonmin, H., Technol, N. K.-Int. J. Eng. T., & 2021, undefined. (n.d.). Review on activated carbon: Synthesis, properties and applications. *Researchgate.Net*. Retrieved September 16, 2025, from https://www.researchgate.net/profile/Nassereldeen-Kabbashi/publication/354843120_Review_On_Activated_Carbon_Synthesis_Properties_And_Applications/links/618cba6807be5f31b76755c7/Review-On-Activated-Carbon-Synthesis-Properties-And-Applications.pdf

Villabona-Ortíz, A., Ortega-Toro, R., & Tejada-Tovar, C. (2022a). Selective and Competitive Adsorption of Anions in Solution on Porous Adsorbent from Zea mays Steams: Kinetic and Equilibrium Study. *Water (Switzerland)*, *14*(18). https://doi.org/10.3390/W14182906

Volcke, E. I., Solon, K., Comeau, Y., & Henze, M. (2020). Wastewater characteristics. Biological wastewater; principles, modelling and designing.

Vunain, E., & Biswick, T. (2019b). Adsorptive removal of methylene blue from aqueous solution on activated carbon prepared from Malawian baobab fruit shell wastes: Equilibrium, kinetics and thermodynamic studies. *Separation Science and Technology (Philadelphia)*, *54*(1), 27–41. https://doi.org/10.1080/01496395.2018.1504794

Vunain, E., Kenneth, D., & Biswick, T. (2017a). Synthesis and characterization of low-cost activated carbon prepared from Malawian baobab fruit shells by H3PO4 activation for removal of Cu(II) ions: equilibrium. *SpringerE Vunain, D Kenneth, T BiswickApplied Water Science, 2017•Springer*, *7*(8), 4301–4319. https://doi.org/10.1007/S13201-017-0573-X

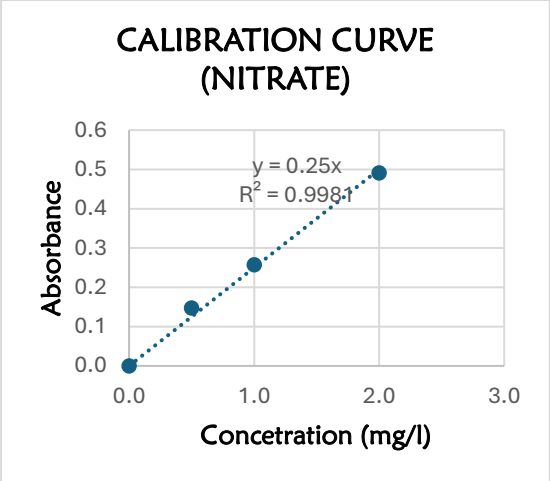
Wang, L., Xu, Z., Fu, Y., Chen, Y., Pan, Z., Wang, R., & Tan, Z. (2018). Comparative analysis on adsorption properties and mechanisms of nitrate and phosphate by modified corn stalks. *RSC Advances*, *8*(64), 36468–36476. https://doi.org/10.1039/C8RA06617E

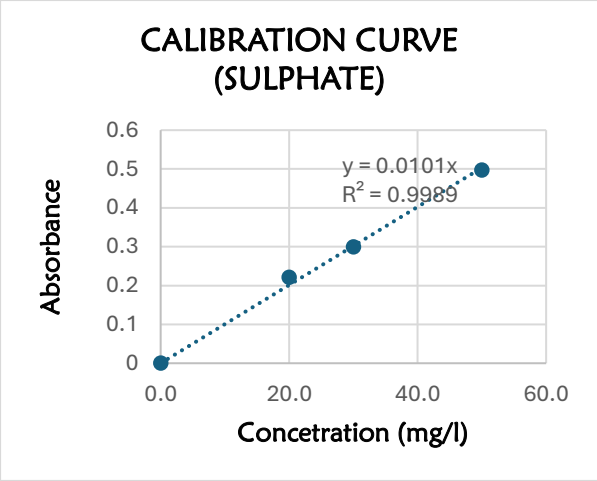
Zeng, W., Loi, Q. k., Shi, J., & Liu, L. (2024, september 1). understanding water adsorption in hierarchical carbon-the significance of pore connectivity and functional group configuratins. *371*.

Zhao, L., Cao, X., Zheng, W., Wang, Q., & Yang, f. (2015, octobe). Endogenous minerals have influences on surface electrochemistry and ion exchange properties of biochar. doi:10.1016/j.chemosphere.2015.04.053

APPENDIX

APPENDIX A: CALIBRATION CURVES





(a) (b)

Figure 13: calibration curve for (a) nitrate and (b) sulphate

APPENDIX B: RAW EXPERIMENTAL DATA (BFS-AC)

B1: Effect of solution pH on Nitrate Removal

Table 24: results on effect of solution pH on NO3- removal

Ph	CONC.(mg/l) Trial 1	CONC.(mg/l) Trial 2	Removal % Trial 1	Removal % Trial 2	Average removal %
Initial concentration	0.400	0.416	0.00	0.00	0.00
2	0.080	0.076	80.00	81.73	80.88
4	0.152	0.172	62.00	58.65	60.29
6	0.180	0.188	55.00	54.81	54.90
7	0.212	0.192	47.00	53.85	50.49
8	0.220	0.244	45.00	41.35	43.14

B2: Effect of solution pH on Sulphate

Table 25: results on effect of solution pH on SO42- removal

pH	CONC.(mg/l) Trial 1	CONC.(mg/l) Trial 2	Removal % Trial 1	Removal % Trial 2	Average removal %
Initial concentration	49.010	48.020	0.00	0.00	0.00
2	35.149	34.653	28.28	27.84	28.79
4	34.158	33.663	30.30	29.90	30.30
6	33.168	32.673	32.32	31.96	32.32
7	29.208	29.208	40.40	39.18	40.40
8	36.139	36.139	26.26	24.74	26.26

B3: Effect of adsorbent dosage Nitrate removal

Table 26: results on effect of adsorbent dosage on NO3- removal

DOSSAGE (g)	CONC.(mg/L) Trial 1	CONC.(mg/L) Trial 2	REMOVAL % Trial 1	REMOVAL % Trial 2	Average removal %
Initial	0.408	0.408	0.00	0.00	0.00
1	0.180	0.188	55.88	53.92	54.90
2	0.048	0.040	88.24	90.20	89.22
3	0.228	0.236	44.12	42.16	43.14
4	0.256	0.240	37.25	41.18	39.22
5	0.292	0.296	28.43	27.45	27.94

B4: Effect of adsorbent dosage on Sulphate

Table 27: results on effect of adsorbent dosage on SO42- removal

Dosage(g)	CONC.(mg/l) Trial 1	CONC.(mg/l) Trial 2	Removal % Trial 1	Removal % Trial 2	Average removal %
Initial concentration	49.80	50.10	0.00	0.00	0.00
1	30.00	32.80	39.76	34.53	34.53
2	13.80	13.90	72.29	72.26	73.05
3	13.00	13.40	73.90	73.25	73.25
4	12.20	12.10	75.50	75.85	75.85
5	14.80	14.40	70.28	71.26	71.36

B5: Effect of contact time on Nitrate removal

Table 28: results on effect of adsorbent dosage on NO_3^- removal

Contact time (min)	CONC.(mg/l) Trial 1	CONC.(mg/l) Trial 2	Removal% Trial 1	Removal% Trial 2	Average removal%
Initial conc	0.392	0.404	0.00	0.00	0.00
30.0	0.248	0.240	36.73	40.59	38.69
60.0	0.040	0.048	89.80	88.12	88.94
90.0	0.032	0.044	91.84	89.11	90.45
120.0	0.084	0.072	78.57	82.18	80.40
180.0	0.164	0.152	58.16	62.38	60.30

B6: Effect of contact time on Sulphate removal

Table 29: results on effect of contact time on SO_4^{2-} removal

Contact time (min)	CONC.(mg/l) Trial 1	CONC.(mg/l) Trial 2	Removal % Trial 1	Removal % Trial 2	Average removal %
Initial concentration	46.075	46.916		0	0.00
30.0	24.299	26.355		43.82	47.26
60.0	8.037	8.318		82.27	82.56
90.0	5.514	5.514		88.25	88.03
120.0	8.692	8.879		81.08	81.14
180.0	10.000	10.280		78.09	78.30

APPENDIX C: RAW EXPERIMENTAL DATA (Raw-BF)

C1: Characterisation of Raw baobab adsorbent

Table 30: moisture content of RB

No	Crucible weight	Initial mass of AC	Final mass (crucible + AC)	Final AC mass	Moisture weight	Moisture content%
1	24.594	1.0055	25.41	0.8161	0.1894	18.8
2	24.848	1.5033	26.07	1.2216	0.2817	18.7
AVERAGE						18.8

Table 31: Volatile matter content of RB

Crucible weight	Initial mass of AC	Final mass	AC final mass	VM weight	Volatile matter %
44.208	5.004	46.401	2.1931	2.8109	56.17

Table 32: Iodine number of RB

sample volume	initial V of T(ml)	final V of T	T used (ml)	iodine number(mg/g)
20	0	18.2	18.2	0.00
20	18.2	35.43	17.23	123.10
20	32.4	49.89	17.49	90.10
20	0	16.99	16.99	153.56
		AVERAGE		122.25

C2: Effect of solution pH on NO_3^- and SO_4^{2-} removal

Table 33: results on effect of solution pH on NO_3^- and SO_4^{2-} removal

pH	NO_3^- conc (mg/l)	SO_4^{2-} conc (mg/l)	Removal% (NO_3^-)	Removal%(SO_4^{2-})
Initial Conc	0.408	50.0	0.00	0.00
2	0.22	36.134	45.6	27.73
4	0.24	41.597	40.4	16.81
6	0.30	42.437	26.2	15.13
7	0.32	44.538	22.2	10.92
8	0.34	45.378	16.4	9.24

C3: Effect of adsorbent dosage on NO_3^- and SO_4^{2-} removal

Table 34: effect of adsorbent dosage on NO_3^- and SO_4^{2-} removal

Dosage(g)	NO_3^- conc (mg/l)	SO_4^{2-} conc (mg/l)	Removal% (NO_3^-)	Removal%(SO_4^{2-})
Initial Conc	0.408	50.0	0.00	0.00
1	0.291	46.64	28.68	6.72
2	0.259	35.295	36.44	29.41
3	0.278	42.44	31.8	15.13
4	0.326	44.96	20.08	10.08
5	0.359	47.48	12.08	5.04

C4: Effect of contact time on NO_3^- and SO_4^{2-} removal

Table 35: effect of contact time on NO_3^- and SO_4^{2-} removal

Time (min)	NO_3^- conc (mg/l)	SO_4^{2-} conc (mg/l)	Removal% (NO_3^-)	Removal%(SO_4^{2-})
Initial Conc	0.408	50.0	0.00	0.00
30	0.359	46.219	12.08	7.563
60	0.325	44.118	20.44	11.765
90	0.246	32.983	39.8	34.034
120	0.249	33.529	38.88	32.941
180	0.262	35.084	35.68	29.832

APPENDIX D: STATISTICAL ANALYSIS (BFS-AC)

D1: Correlation Results

Table 36: correlation on effect of solution pH

	pH	*Sulphate (% Removal)*	*Nitrate (% Removal*
pH	1		
Sulphate (% Removal)	0.23	1	
Nitrate (% Removal	-0.97	-0.183	1

Table 37: correlation on effect of adsorbent dosage

	Dosage (g)	*Sulphate (% Removal*	*Nitrate (% Removal)*
Dosage (g)	1		
Sulphate (% Removal	0.69	1	
Nitrate (% Removal)	-0.70	-0.092	1

Table 38: correlation on effect of adsorbent dosage

	Contact time (min)	*Sulphate (% Removal)*	*Nitrate (% Removal*
Contact time (min)	1		
Sulphate (% Removal)	0.515937919	1	
Nitrate (% Removal	0.136867268	0.91463029	1

D2: ANOVA results

Effect of solution pH

Anova: Single Factor

SUMMARY

Groups	*Count*	*Sum*	*Average*	*Variance*
Ph	*5*	*27*	*5.4*	*5.8*
Sulphate (% Removal)	*5*	*158.082*	*31.6164*	*29.02863*
Nitrate (% Removal	*5*	*289.7059*	*57.94118*	*203.936*

ANOVA

Source of Variation	*SS*	*df*	*MS*	*F*	*P-value*	*F crit*
Between Groups	*6901.448*	*2*	*3450.724*	*43.35723*	*3.23E-06*	*3.885294*
Within Groups	*955.0585*	*12*	*79.58821*			
Total	*7856.506*	*14*				

Effect of adsorbent dosage

Anova: Single Factor

SUMMARY

Groups	*Count*	*Sum*	*Average*	*Variance*
Dosage (g)	*5*	*15*	*3*	*2.5*
Sulphate (% Removal	*5*	*328.043 9*	*65.6087 8*	*304.399 2*
Nitrate (% Removal)	5	254.4118	50.8823 5	551.9992

ANOVA

Source of Variation	*SS*	*df*	*MS*	*F*	*P-value*	*F crit*
Between Groups	10715.75	2	5357.87 3	18.71422	0.00020 5	3.88529 4
Within Groups	3435.59 4	12	286.299 5			
Total	14151.34	14				

Effect of contact time

Anova: Single Factor

SUMMARY

Groups	*Count*	*Sum*	*Average*	*Variance*
Contact time (min)	*5*	*480*	*96*	*3330*
Sulphate (% Removal)	*5*	*375.384 1*	*75.0768 2*	*285.933 3*
Nitrate (% Removal	*5*	*358.794*	*71.75879*	*486.0231*

ANOVA

Source of Variation	*SS*	*Df*	*MS*	*F*	*P-value*	*F crit*
Between Groups	1727.374	2	863.6872	0.631665	0.54849 4	3.88529 4
Within Groups	16407.8 3	12	1367.319			
Total	18135.2	14				

APPENDIX E: Experimental Photographs

E1: production of BFS-AC



(a)



(b)

Figure 14: stages in BFS-AC production, (a) drying of shells impregnated in acid, (b) Muffle furnace used for carbonization at 700°C

E2: characterisation and batch adsorption experiment



(a)



(b)

Figure 15: characterisation and adsorption experiment respectively, (a) iodine number test, (b) measuring final SO42- concentration after adsorption experiment using UV/VIS Spectrophotometer